most reasonably attributed to a rotational isotope effect,[11] is consistent with concert. For the isotope effect to be consistent with the stereospecific biradical pathway, closure to the five-membered ring must be rate-determining. However, it is hard to reconcile the demand of slow closure to a five-membered ring relative to closure to a three-membered ring with the demand of rapid closure to a five-membered ring relative to bond rotation in the diradical. Thus, the 1,3-shift would appear to be concerted.

Acknowledgment. We thank the National Science Foundation for financial support, Prof. Christopher Samuel (U. Warwick), who provided the initial NMR data and spectral analysis of the product epoxide to warrant pursuit of this work, and Prof. Kevin Gilbert for his continued interest in this problem.

Supplementary Material Available: Experimental details for the synthesis of **1** and NMR spectra of the methylene protons of the undeuterated epoxide, the deuterated epoxide from the three different reaction times, and simulations of mixtures (9 pages). Ordering information is given on any current masthead page.

(11) Dai, S. H.; Dolbier, J. *J. Am. Chem. Soc.* **1970**, *92*, 1774; **1972**, *94*, 3946. Crawford, R. J.; Chang, M. H. *Tetrahedron* **1982**, *38*, 837. Gajewski, J. J.; Benner, C. W.; Stahly, B. N.; Hall, R. F.; Sato, R. I. *Tetrahedron* **1982**, *38*, 853.

Atomic Structure of the Rapamycin Human Immunophilin FKBP-12 Complex

Gregory D. Van Duyne,† Robert F. Standaert,‡ Stuart L. Schreiber,*,‡ and Jon Clardy*,†

Department of Chemistry, Cornell University Ithaca, New York 14853
Department of Chemistry, Harvard University Cambridge, Massachusetts 02138

Received June 3, 1991

Complexes of immunophilins with immunosuppressive drugs interfere with a variety of signal transduction pathways in the cytoplasm of the cell.[1-3] Rapamycin[4] (**1**) is a high affinity ligand (K_d = 0.2 nM)[2] to the immunophilin FKBP-12[5-7] and appears to be a general and potent antiproliferative agent.[1] The pleiotropic actions of rapamycin on growth factor receptor signaling pathways have elevated this compound to a high status as a probe of signaling mechanisms. Although the precise details have yet to be elucidated, the *complex* of human FKBP-12 and rapamycin has been shown by genetic methods to function as the inhibitory agent.[8] Herein we report the three-dimensional structure of the complex of human FKBP-12 and rapamycin, determined to 1.7-Å resolution

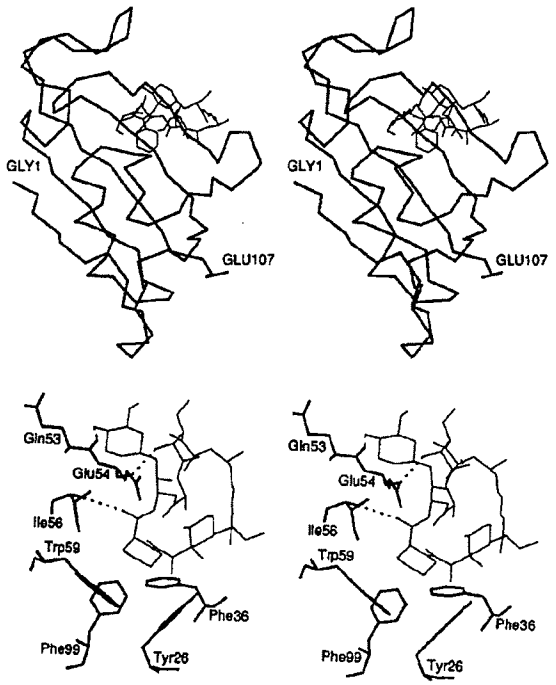

Figure 1. (a, top) A stereoview of the α-carbon tracing of FKBP-12 and rapamycin. The N- and C-terminal α-carbons are labeled. (b, bottom) A stereodrawing of the binding pocket showing all of the bound rapamycin molecule and selected FKBP-12 residues.

by X-ray crystallographic techniques.[9] This structure provides a framework to interpret the effects of structural perturbation of either rapamycin or human FKBP-12 on signal transduction pathways.

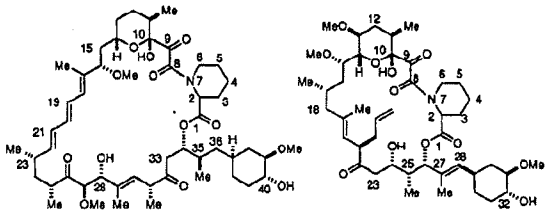

As shown in Figure 1, the protein component of the FKBP-12/rapamycin complex forms a five-stranded antiparallel β-sheet

†Cornell University.
‡Harvard University.

(1) Schreiber, S. L. *Science* **1991**, *251*, 283.
(2) Bierer, B. E.; Matila, P. S.; Standaert, R. F.; Herzenberg, L. A.; Burakoff, S. J.; Crabtree, G.; Schreiber, S. L. *Proc. Natl. Acad. Sci. U.S.A.* **1990**, *87*, 9231–9235.
(3) Bierer, B. E.; Somers, P. K.; Wandless, T. J.; Burakoff, S. J.; Schreiber, S. L. *Science* **1990**, *250*, 556–559.
(4) Findlay, J. A.; Radics, L. *Can. J. Chem.* **1980**, *58*, 579.
(5) The family of proteins that bind to FK506 and rapamycin have been collectively named FKBP's (FK506 binding proteins), with a suffix designating the approximate molecular weight. Human FKBP-12, the most abundant FKBP found in the cytoplasm, is a 12 kD protein of 107 amino acids that binds FK506 and rapamycin and catalyzes the cis–trans isomerization of peptidyl–prolyl amide bonds in peptide substrates.
(6) Harding, M. W.; Galat, A.; Uehling, D. E.; Schreiber, S. L. *Nature* **1989**, *341*, 758.
(7) Siekierka, J. J.; Hung, S. H. Y.; Poe, M.; Lin, C. S.; Sigal, N. H. *Nature* **1989**, *341*, 755.
(8) Koltin, Y.; Faucette, L.; Bergsma, D. J.; Levy, M. A.; Cafferkey, R.; Koser, P. L.; Johnson, R. K.; Livi, G. P. *Mol. Cell. Biol.* **1991**, *11*, 1718.

(9) Crystals of the FKBP-12/rapamycin complex were grown from solutions containing 10 mg/mL of protein complex, 300 mM ammonium sulfate, and 100 mM phosphate at pH 6.0 using the hanging drop method at room temperature. The space group is $P2_12_12_1$ with a = 45.42 Å, b = 49.16 Å, c = 54.74 Å, and one molecule in the asymmetric unit. Data were measured using a SanDiego Multiwire Systems Mark II detector and a rotating anode source to 1.7-Å resolution. A total of 81 484 reflections were measured (12 991 unique, 93% complete, R_{sym} = 0.056, 10 633 with $F \geq 3\sigma$) from two crystals. The structure was solved using the molecular replacement method with a search model composed of the protein component of the FKBP-12/FK506 complex and the MERLOT program system.[10] The structure was refined with X-PLOR[11] using least-squares minimization by conjugate gradients where the stereochemical restraints used in ligand refinement were restricted to terms for bond lengths, bond angles, and improper dihedral angles (for planar sp^2 carbons and chiral centers). The conformation of bound rapamycin was determined unambiguously from well-defined electron density in $2F_o-F_c$ maps. The R factor for the current model, including FKBP-12, rapamycin, and 85 water molecules, is 0.165. All main chain atoms, all buried side-chain atoms, and all ligand atoms are well-defined in the final $2F_o - F_c$ electron density map. The root-mean-square deviations of bond lengths and bond angles from their ideal values are 0.01 Å and 2.8°, respectively.
(10) Fitzgerald, P. M. D. *J. Appl. Crystallogr.* **1988**, *21*, 273.
(11) Brünger, A. T. *X-PLOR Manual, Version* 2.1; Yale University, New Haven, 1990.

0002-7863/91/1513-7433$02.50/0

wrapping with a right-handed twist around a short α-helix—the same folding topology found in the complex of FKBP-12 with FK506[12] and in uncomplexed FKBP-12.[13,14] The root-mean-square (rms) deviations of α-carbons, backbone atoms, and all protein atoms between FKBP-12 complexed with rapamycin and FKBP-12 complexed with FK506 are 0.67, 0.67, and 1.51 Å, respectively. Only one region, involving residues 31–34 in the loop between strands 4 and 5 of the β-sheet structure, adopts a different main chain conformation. These residues are not involved in protein–ligand interactions, but may be important recognition features of the complex.

Rapamycin binds in a cavity between the β-sheet and α-helix with the pipecolinyl ring deeply buried in the protein (Figure 1a). The protein–ligand interface involves atoms from the pyranose ring through the C28 hydroxyl, with the remainder, including the C17-C22 triene, exposed. The C1 ester, the pipecolinyl ring, the C8 and C9 carbonyls, and the pyranose ring adopt a conformation that is superimposable with the same groups in the FKBP-12/FK506 complex.[12] Three hydrogen bonds between this region and FKBP-12 (Ile-56 NH to C1 carbonyl, Tyr-82 hydroxyl to C8 carbonyl, and Asp-37 carboxylate to C10 hydroxyl) and a C9 carbonyl binding pocket involving C–H···O interactions with α-hydrogens from Tyr-26, Phe-36, and Phe-99 are also identical with those found in the complex with FK506, thus confirming the identical binding roles of the common structural elements[15] in the two immunosuppressant ligands.

Two additional hydrogen bonds are involved in rapamycin binding to FKBP-12 (Figure 1b). The first is from Glu-54 main chain carbonyl to C28 hydroxyl, which along with the Ile-56 NH to C1 carbonyl–hydrogen bond may mimic the interaction of the dipeptide portion of a natural substrate with FKBP-12. It has been noted that the pyranose–pipecolinyl region also mimics a dipeptide,[16] making rapamycin, like FK506, a possible example of an extended peptide mimic. This hydrogen bond is analogous to the one from Glu-54 main chain carbonyl to C24 hydroxyl found in the FKBP-12/FK506 complex.[12] The second hydrogen bond is from Gln-53 main chain carbonyl to the C40 hydroxyl. In the rapamycin complex the cyclohexyl group (C35–C42) is bound to the protein through this hydrogen bond, while the FK506 complex has no such cyclohexyl–protein interaction. FK506's (2) C27–C28 double bond restricts the orientations of the cyclohexane while in rapamycin (1) the cyclohexyl ring can swing about the C35–C36 bond to form a Gln-53 carbonyl to C40 hydroxyl hydrogen bond.

The conformation of bound rapamycin is virtually identical with that seen in the free, crystalline state,[4] with an rms difference of 0.49 Å. Unlike FK506, which undergoes a cis to trans isomerization of the amide bond accompanied by a dramatic change in overall conformation on binding to FKBP-12,[12] rapamycin possesses a high degree of structural preorganization for binding. This preorganization, along with the anchoring of the cyclohexyl group, may explain the twofold higher affinity (K_d = 0.2 nM) of rapamycin for FKBP-12 compared to FK506 (K_d = 0.4 nM).[2]

The view of the FKBP-12/rapamycin complex as the biological effector in immunosuppressive function requires a focus on the complex as a whole—in particular the exposed regions of bound rapamycin and the FKBP-12 loops flanking the binding site. The likely role of FKBP-12 and other FKBP's in the disruption of signal transduction in T-cells is to present rapamycin (or FK506) to as yet unknown biological acceptors, or partner proteins. The FKBP-12/rapamycin complex described may be best viewed in this context as the ligand, now known at atomic resolution, to a partner protein involved in cytoplasmic signal transduction.

Acknowledgment. We thank T. J. Stout and P. A. Karplus for technical assistance and Walt Cullen and Jack Oscarson of the National Products Discovery and Fermentation Department at Pfizer, Inc. for supplying the rapamycin used in this study. Support from the National Cancer Institute (CA-24487, J.C.) and the National Institute of General Medical Sciences (GM-38627, S.L.S.) is gratefully acknowledged. The area detector facility was supported by NSF Grant DIR-8820910. Coordinates of the bound rapamycin molecule are available from the authors. The complete refined coordinates of the FKBP-12/rapamycin complex will be deposited in the Brookhaven Protein Databank.

Self-Assembling, Alkali-Metal-Complexing Nickel Salicylaldimine Complexes

Otto F. Schall, Kerry Robinson,† Jerry L. Atwood,† and George W. Gokel*

Departments of Chemistry, University of Miami Coral Gables, Florida 33124
University of Alabama, University, Alabama 35487-0336
Received May 23, 1991

Nature often achieves biological function in large molecules that are shaped and ordered by various feeble forces such as hydrogen bonding, salt-bridge formation, π-stacking, etc. We[1] and others[2] have been interested in this phenomenon especially from the perspective of developing relatively small molecular hosts that can assemble, organize, and bind. This phenomenon has two manifestations that should be distinguished, however. On the one hand, there are those that self-assemble to bind with little structural change.[3] On the other, there are hosts such as carboxypeptidase A that undergo significant structural change ("induced-fit system") when a guest is bound.[4] A model in the former category was devised by Reinhoudt et al., who used a macrocyclic salen–polyether–UO_2 complexes to afford a binding site for urea.[5] We now report an unusual nickel salicylaldimine system that was thought[6] to be in the former category but actually forms an unusual bimetallic molecular cage.

3-Hydroxysalicylaldehyde was converted into a series of 3-alkoxy-*N*-methylsalicylaldimine derivatives as previously described.[6] The side arms in the 3-position included methyl (CH_3, **1**), 2-methoxyethyl ($CH_2CH_2OCH_3$, **2**), and 2-(2-methoxyethoxy)ethyl ($CH_2CH_2OCH_2CH_2OCH_3$, **3**). It is known that such aldimine systems react with nickel to form square-planar nickel(II) complexes of the NiL_2 variety.[7] These complexes may undergo tetrahedral–square planar equilibria if the system is sterically hindered. Some diamagnetic, square-planar complexes further associate by forming paramagnetic dimers.[8] We isolated the complex $\mathbf{1}_2$Ni as previously reported.[6] The combustion analysis and mass spectrum were compatible with the indicated stoichiometry. Assessment of stoichiometry in such cases by vapor pressure osmometry (VPO) has been eschewed as the results do not always accord with those of cryoscopic studies (see supplementary material).[9] Our studies using VPO indicated that $\mathbf{1}_2$Ni

†University of Alabama.

(1) (a) Kim, M.; Gokel, G. W. *J. Chem. Soc., Chem. Commun.* **1987**, 1686. (b) Medina, J. C.; Li, C.; Bott, S. G.; Atwood, J. L.; Gokel, G. W. *J. Am. Chem. Soc.* **1991**, *113*, 367. (c) Gokel, G. W.; Medina, J. C.; Li, S. *Synlett*, in press.
(2) (a) Rebek, J., Jr. *Top. Curr. Chem.* **1988**, *149*, 189. (b) Shinkai, S.; Miyazaki, K.; Manabe, O. *J. Chem. Soc., Perkin Trans. 2* **1987**, 449.
(3) Hamilton, A. *Adv. Supramolecular Chem.* **1990**, *1*, 1.
(4) (a) Hartsuck, J. A.; Lipscomb, W. N. *Enzymes* **1971**, *3*, 1. (b) Quiocho, F. A.; Lipscomb, W. N. *Adv. Protein Chem.* **1971**, *25*, 1. (c) Lipscomb, W. N. *Proc. Natl. Acad. Sci. U.S.A.* **1980**, *77*, 3875.
(5) Van Staveren, C. J.; van Erden, J.; van Veegel, C. J. M.; Harkema, S.; Reinhoudt, D. N. *J. Am. Chem. Soc.* **1988**, *110*, 4994–5008.
(6) Schepartz, A.; McDevitt, J. *J. Am. Chem. Soc.* **1989**, *111*, 5976.
(7) (a) Holm, R. H.; Everett, G. W., Jr.; Chakravarty, A. *Prog. Inorg. Chem.* **1966**, *7*, 83. (b) Holm, R. H.; O'Connor, M. J. *Prog. Inorg. Chem.* **1971**, *14*, 241.
(8) Holm, R. H. *J. Am. Chem. Soc.* **1961**, *83*, 4683.
(9) (a) Holm, R. H.; Swaminathan, K. *Inorg. Chem.* **1962**, *1*, 599. (b) Holm, R. H.; Swaminathan, K. *Inorg. Chem.* **1963**, *2*, 181.
(12) Van Duyne, G. D.; Standaert, R. F.; Karplus, P. A.; Schreiber, S. L.; Clardy, J. C. *Science* **1991**, *252*, 839.
(13) Michnick, S. W.; Rosen, M. K.; Wandless, T. J.; Karplus, M.; Schreiber, S. L. *Science* **1991**, *252*, 836.
(14) Moore, J. M.; Peattie, D. A.; Fitzgibbon, M. J.; Thomson, J. A. *Nature* **1991**, *351*, 248.
(15) Wandless, T. J.; Michnick, S. W.; Rosen, M. K.; Karplus, M.; Schreiber, S. L. *J. Am. Chem. Soc.* **1991**, *113*, 2339.
(16) Albers, M. W.; Walsh, C. T.; Schreiber, S. L. *J. Org. Chem.* **1990**, *55*, 4984.

0002-7863/91/1513-7434$02.50/0

J. Mol. Biol. (1993) 229, 105–124

Atomic Structures of the Human Immunophilin FKBP-12 Complexes with FK506 and Rapamycin

Gregory D. Van Duyne[1], Robert F. Standaert[2], P. Andrew Karplus[3] Stuart L. Schreiber[2] and Jon Clardy[1]

[1]*Department of Chemistry, Cornell University Ithaca, NY 14853-1301, U.S.A.*

[2]*Department of Chemistry, Harvard University Cambridge, MA, U.S.A.*

[3]*Department of Biochemistry, Cornell University Ithaca, NY 14853, U.S.A.*

(Received 3 January 1992; accepted 29 July 1992)

High resolution structures for the complexes formed by the immunosuppressive agents FK506 and rapamycin with the human immunophilin FKBP-12 have been determined by X-ray diffraction. FKBP-12 has a novel fold comprised of a five-stranded β-sheet wrapping around a short α-helix with an overall conical shape. Both FK506 and rapamycin bind in the cavity defined by the β-sheet, α-helix and three loops. Both FK506 and rapamycin bind in similar fashions with a set of hydrogen bonds and an unusual carbonyl binding pocket. Bound FK506 has a different conformation than free (crystalline) FK506 while rapamycin's bound conformation is virtually identical to that of unbound rapamycin. FKBP-12 is a peptidyl-prolyl isomerase (PPIase), and the structures of the complexes suggest ways in which this catalytic activity could operate. The different complexes are active in suppressing different steps of T cell activation, an activity seemingly unconnected with the PPIase activity.

Keywords: FKBP; immunophilin; immunosuppression; FK506; rapamycin

1. Introduction

The natural products FK506 and rapamycin have tremendous attraction both as templates for immunosuppressive drugs and as probe molecules for cytoplasmic signal transduction. Like cyclosporin A, currently the clinically favored agent for the prevention of graft rejection after organ and bone marrow transplantation, FK506 and rapamycin inhibit T cell activation (Schreiber, 1991). FK506 has a mechanism of action similar to that of cyclosporin A, but is 10 to 100 times more potent (Thomson, 1989). Rapamycin inhibits T cell activation at concentrations comparable to those of structurally related FK506, but at a different stage and by a different mechanism (Metcalf & Richards, 1990).

A key step in signal disruption is the binding of the drug to a protein, and in this paper we discuss the detailed structures of two such complexes. The predominant FK506-binding protein in Jurkat T cells, termed FKBP and later named FKBP-12 to distinguish it from other FKBPs by its molecular weight, was isolated and characterized by two laboratories (Harding *et al.*, 1989; Siekierka *et al.*, 1989). FKBP-12 is a 12 kDa protein of 107 residues that binds both FK506 and rapamycin tightly, with dissociation constants $K_d = 0{\cdot}4$ and $0{\cdot}2$ nM, respectively (Bierer *et al.*, 1990*a*). A number of other, less abundant FKBPs have since been characterized (Jin *et al.*, 1991; Fretz *et al.*, 1991). Cyclophilin A, an 18 kDa protein with no sequence similarity to FKBP-12, is the predominant cyclosporin-binding protein in T lymphocytes and was shown to be identical to peptidyl-prolyl isomerase, an enzyme that catalyzes the interconversion of *cis*- and *trans*-rotamers of the peptidyl-prolyl amide bond of peptide and protein substrates. Cyclosporin potently inhibits this rotamase activity (Fischer *et al.*, 1989; Takahashi *et al.*, 1989). FKBP-12 is also a rotamase and its rotamase activity is potently inhibited by both FK506 and rapamycin.

FK506 and cyclosporin have been shown to suppress T cell activation by disruption of the cyto-

0022-2836/93/010105-20 $08.00/0

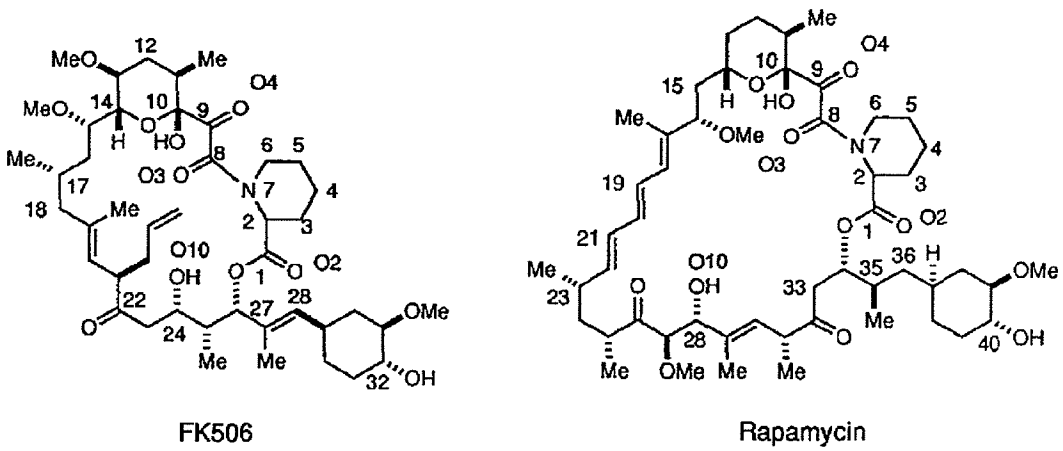

Figure 1. Structures of FK506 and rapamycin.

plasmic signal transduction process resulting from stimulation of the T cell receptor (TCR†) by foreign antigen. The TCR pathway results in the activation of specific nuclear transcription factors such as nuclear factor of activated T cells (NF-AT), and these factors then regulate the transcription of T cell activation genes such as that for lymphokine interleukin-2 (IL-2). Rapamycin does not inhibit the TCR pathway and has no effect on IL-2 production. Rather it inhibits T cell response to IL-2, indicating its involvement with a later, lymphokine receptor-associated pathway.

Inhibition of FKBP-12's rotamase activity is an insufficient requirement for T cell suppression, as proved by the distinct modes of action of FK506 and rapamycin, the observation that FK506 and rapamycin are mutually inhibitory (Bierer *et al.*, 1990*a*), and the inability of 506BD, a synthetic tight binder and rotamase inhibitor containing the binding domains of FK506 and rapamycin, to affect signal transduction (Bierer *et al.*, 1990*b*). For both FK506 and rapamycin, the biological effectors in blocking cytoplasmic signal transduction are the FKBP-12–FK506 and FKBP-12–rapamycin complexes. Whether these complexes are viewed as rotamase–inhibitor complexes or as biological effectors that interact with a third component, a high resolution structure would be of enormous value.

In two preliminary reports, we have described the structures of the FKBP-12–FK506 and FKBP-12–rapamycin complexes following initial refinement at 1·7 Å (1 Å = 0·1 nm) resolution (Van Duyne *et al.*, 1991*a*,*b*). The solution structure of uncomplexed FKBP-12 has also been determined by n.m.r. techniques (Michnick *et al.*, 1991; Moore *et al.*, 1991). In all cases, the protein fold is the same, a five-stranded β-sheet wrapped around a short α-helix with the overall shape of an empty ice cream cone (Fig. 2(a)). FK506 and rapamycin bind in a hydrophobic cavity between the helix and sheet that is flanked by three loop regions. Here we report the refined, 1·4 Å resolution structure of FKBP-12–FK506 and the 1·7 Å structure of FKBP-12–rapamycin. Structural features of the protein include: a novel β-sheet loop crossing, a split β-sheet strand containing an eight-residue insertion that forms a large bulge in the sheet, and an unusual 20-residue loop that acts as a flap over the ligand binding region. Features of ligand binding include: a twisted dicarbonyl involved in C–H···O interactions, a planar, *trans*-amide, and different cyclohexyl group orientations. Although the protein–ligand interactions observed do not lead unambiguously to a mechanism of rotamase action, they do provide some tantalizing possibilities. Differences between the two complexes provide a starting point for understanding the nature of the immunophilin–immunosuppressant complex receptor and for the design of new biological probes based on the FK506 and rapamycin structures.

2. Materials and Methods

(a) *FKBP-12 and selenomethionine FKBP-12*

Selenomethionine-labeled FKBP-12 (SeMet-FKBP-12) was expressed using the same vector (pHNJ+) and host strain (*Escherichia coli* XA90) under modified conditions, and it was purified by a similar protocol. As XA90 is not a methionine auxotroph, the conditions were chosen to exclude methionine from the medium and to provide ample amounts of other amino acids known to inhibit methionine biosynthesis. Thus, cells from 1 ml of an overnight culture grown in LB medium containing 100 mg of ampicillin/l were isolated by centrifugation (2 min at 1300 *g* in a microcentrifuge), resuspended in 1 ml of M9 minimal medium containing glucose (0·4%, w/v) and ampicillin (100 mg/l), and added to 1 l of the same medium pre-warmed to 37 °C. The culture was shaken in a

† Abbreviations used: TCR, T cell receptor; NF-AT, nuclear factor of activated T cells; IL-2, interleukin-2; n.m.r., nuclear magnetic resonance; SeMet-FKBP-12, selenomethione-labeled FKBP-12; DTT, dithiothreitol; m.i.r., multiple isomorphous replacement; r.m.s., root-mean-square.

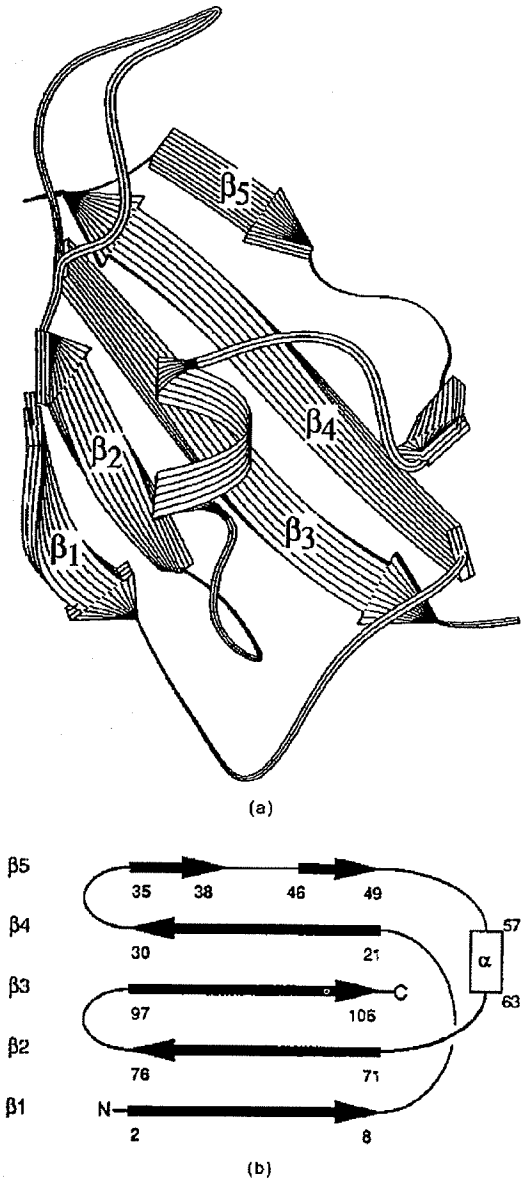

Figure 2. (a) Ribbon and (b) topological representations of FKBP-12.

4-l Morton flask at 37°C until it had reached an A_{600} of 0·6, at which point selenomethionine (Sigma, 50 mg) along w th lysine hydrochloride (100 mg), threonine (100 mg), phenylalanine (100 mg), leucine (50 mg), isoleucine (50 mg) and valine (50 mg) were added as solids. After an additional 15 min of shaking, 10 ml of 100 mM-isopropyl-β-D-thiogalactoside was added, and the culture was grown for 13 h more. The cells were harvested by centrifugation (15 min, 500 *g*), washed by suspension in ~25 ml of lysis buffer (20 mM-Tris·HCl, 2 mM-EDTA, 10^{-7} M-pepstatin A 5 mM-DTT, pH 8·0 at 22°C) followed by centrifugation, suspended again in 25 ml of lysis buffer, and lysed by sonication. Protamine sulfate (5 ml of a 2% solution, pH 7·5) was added, and the mixture was incubated on ice for 30 min prior to centrifugation (37,000 *g*, 30 min). The supernatant was chromatographed at 4°C on a 2·5 cm × 15 cm column of DE-52 (Whatman) equilibrated with 20 mM-Tris·HCl, 5 mM-DTT (pH 8·0) at 22°C and eluted with the same buffer. FKBP-12 eluted in the first peak detected by A_{280}. Fractions were analyzed by SDS-PAGE followed by Coomassie blue staining, and FKBP-12-containing fractions were combined, concentrated to 1 to 2 ml using a stirred cell with an Amicon YM-3 membrane, and chromatographed at 4°C on a 1·6 cm × 70 cm column of Sephacryl S-100 (Pharmacia) equilibrated with 20 mM-Tris·HCl, 1 mM-EDTA, 5 mM-DTT (pH 8·0) at 22°C. Fractions were analyzed by SDS-PAGE followed by silver staining, and appropriate fractions were pooled and concentrated using a Centricon-3 microconcentrator (Amicon). A yield of 10 mg of purified SeMet-FKBP-12 was obtained (determined by A_{280} using the extinction coefficient of 9860 M^{-1} cm^{-1} calculated for FKBP-12), and the SeMet incorporation was estimated to be 80 to 85% on the basis of residual methionine content in the amino acid analysis (Yang *et al.*, 1990).

(b) *Crystallizations*

Tetragonal prisms of FKBP-12–FK506 complex measuring up to 0·3 mm along the unique axis and 0·5 mm in width were grown in 5 to 7 days from 10 μl hanging drops containing 10 mg/ml FKBP-12–FK506 complex, 100 mM-phosphate, 1·6 to 1·8 M-ammonium sulfate, (pH 6·0) at room temperature. Crystal data are given in Table 1. Selenomethionine FKBP-12–FK506 crystals were grown under the same conditions and have identical cell constants.

Thin needles of FKBP-12–rapamycin were grown from 10 μl hanging drops containing 10 mg/ml FKBP-12–rapamycin complex, 100 mM-phosphate, 0·4 M-ammonium sulfate (pH 6·0) at room temperature. The needles typically measured less than 100 μm in width and greater than 1 mm in length and were not suitable for high resolution data collection. Improved crystals were grown from 100 mM-phosphate, 0·3 M-ammonium sulfate (pH 6) using a combination of microscopic (McPherson, 1976) and macroscopic (Thaller *et al.*, 1981) seeding techniques. Thin needles were crushed with the end of a glass rod, diluted to 100 μl with reservoir solution, and used as micro-seeds by adding 0·2 μl of seed solution to a hanging drop that was pre-equilibrated at 0·3 M-ammonium sulfate. Large numbers of small crystals grew in 5 days. Suitable crystals were chosen from this crop, washed, and used as macroscopic seeds, 1/pre-equilibrated 10 μl hanging drop. Crystals with maximum dimensions 0·3 mm × 0·3 mm × 1·0 mm grew in 10 to 14 days. Attempts to grow large single crystals using microscopic seeding alone with small numbers of microseeds resulted in only slightly improved crystal axial ratios. Crystal data are given in Table 1.

(c) *Data collection*

Native data were measured to 1·4 Å for the FKBP-12–FK506 complex and to 1·7 Å for the FKBP-12–rapamycin complex using a San Diego Multiwire Systems Mark II detector with graphite-monochromated CuKα radiation produced by a Rigaku RU-200 rotating anode X-ray source operating at 7·5 kW. In both cases, 2 crystals were used. For FKBP-12–FK506, data were

Table 1
Crystal and refinement data

	FKBP-12-FK506	FKBP-12-rapamycin
Cell constants (Å)	$a = 58.07$	$a = 45.42$
		$b = 49.16$
	$c = 55.65$	$c = 54.74$
Space group	$P4_22_12$	$P2_12_12_1$
No. complexes per asymmetric unit	1	1
% Solvent	32	48
No. refined non-hydrogen atoms	1023	1030
Protein	832	832
Ligand	57	65
Solvent	134	133
R-factor (Å)	0.175 (10–1.4)	0.154 (10–1.7)
Final $2F_o-F_c$ map (including $F(000)$) (Å)	25–1.4	25–1.7
Min (e/Å^3)	−0.83	−0.71
Max	6.67	4.15
r.m.s.	0.66	0.55
Final F_o-F_c map (Å)	5–1.4	5–1.7
Min (e/Å^3)	−0.43	−0.24
Max	0.40	0.25
r.m.s.	0.09	0.05
r.m.s. bond deviation (Å)	0.012	0.011
r.m.s. angle deviation (°)	2.6	2.5
r.m.s. improper torsion deviation (°)	1.6	2.0
Average *B* (all atoms) (Å^2)	13.5	20.5
Average *B* (main-chain) (Å^2)	9.0	15.9
Average *B* (ligand) (Å^2)	9.0	13.4
WA (weight for X-ray term in X-PLOR)	48,000	69,000

measured to 1.7 Å with crystal no. 1 and to 1.4 Å with crystal no. 2 and for FKBP-12–rapamycin, data were measured to 1.7 Å for both crystals. Data were measured at room temperature in 30 s frames of width 0.08° in ω, with a crystal-to-detector distance of 340 mm. Data reduction was performed on site (Howard *et al.*, 1985).

Heavy atom derivative and selenomethionine FKBP-12-FK506 data were measured on a Siemens R3m diffractometer using graphite monochromated CuKα radiation from a sealed tube X-ray source operating at 2 kW and 11-step ω-scans, typically 0.75° in width. The $HgCl_2$ and K_2PtCl_4 data were corrected for absorption based on the variation in intensity of 10 azimuthal scans (Siemens Analytical X-ray Instruments, Inc., 1990). The data were also corrected for decomposition (Siemens Analytical X-ray Instruments, Inc., 1990); in all cases less than 10% as judged by the intensities of periodically measured standard reflections. Although high resolution derivative data collection using the area detector system was planned, successful phasing and map interpretation using the preliminary diffractometer data made it unnecessary. Data collection statistics are given in Table 2.

(d) *Multiple isomorphous replacement phasing of FKBP-12-FK506*

Native phases were obtained using the multiple isomorphous replacement (m.i.r.) method, with $HgCl_2$ (bound to Cys22), K_2PtCl_4 (bound to Met29 at site 1 and to Met49 and Lys52 at site 2), and selenomethionine derivatives. Refinement of the heavy atom parameters and calculation of m.i.r. phases were performed with a locally modified version of the program LEASTSQ (Rossmann, 1975). A summary of the heavy atom parameters and phasing statistics for the 3 derivatives used is given in Table 3. The thermal parameters listed for the 3 selenium atoms correlate well with the environments of the corresponding methionine sulfur atoms in the final structure: Met29 and Met49 are surface residues and Met66 is buried. The initial electron density map, calculated with m.i.r. phases at 3.0 Å, was of high quality; the mean figure-of-merit for reflections to 3 Å was 0.63. The entire peptide chain could be traced and many buried side-chains could be identified, with breaks in density occurring only in 2 loop regions. In addition, the entire bound

Table 2
Data collection statistics

Crystal (number used)	Resolution (Å)	Number measured	Number unique	R_{sym}	Percent complete	Number with $F \geq 3\sigma$
FKBP-12-FK506 native (2)	25–1.4	139,003	18,608	0.073	96	17,038
FKBP-12-FK506 $HgCl_2$ (1)	25–3.0	4556	2176	0.066	100	1893
FKBP-12-FK506 K_2PtCl_4 (1)	25–4.0	918	918		97	756
FKBP-12-FK506 Se-Met (1)	25–3.6	1305	1305		100	1140
FKBP-12-rapamycin native (2)	25–1.7	81,484	12,991	0.056	93	10,633

$R_{sym} = \Sigma_{hkl}\Sigma_j|I_j(hkl) - \langle I(hkl)\rangle|/\Sigma_{hkl}\Sigma_j\langle I(hkl)\rangle$, where j runs over symmetry related reflections.

Table 3
Heavy atom parameters and phasing statistics

Derivative	Conc. (mM)	Soak time (days)	Site	Parameters					Resolution (Å)	R_{cul}‡	Phasing power§			
				x	*y*	*z*	*q*†	*B*			6	4	3·5	3
$HgCl_2$	2	3	Hg1	0·358	0·485	0·173	61·3	25·4	3·0	0·23	3·06	2·02	1·86	1·78
K_2PtCl_4	2	6	Pt1	0·612	0·086	0·556	32·2	20·3	3·0	0·13	1·89	1·53		
			Pt2	0·000	0·000	0·313	7·8	35·8						
Se-Met			M29	0·108	0·601	0·443	16·5	28·9	3·6	0·10	2·27	1·71	1·38	
			M49	0·468	0·486	0·157	16·5	40·9						
			M66	0·176	0·510	0·218	16·5	12·1						
Average figures-of-merit											0·84	0·75	0·62	0·45

† Occupancy is given in electrons and is a multiplier for a unit form factor. (Data were placed on an absolute scale following refinement.)
‡ $R_{cul} = \Sigma||F_p - F_{ph}||/\Sigma F_p$, where F_p and F_{ph} are the amplitudes of native and derivative structure factors, respectively.
§ Phasing power = r.m.s. heavy atom scattering amplitude/r.m.s. closure error. Average figures-of-merit are given on the final line. Note that only a single derivative contributes to the phasing beyond 3·5 Å.

FK506 molecule was represented by strong electron density in this first map. The chain tracing was accelerated by the availability of a model of uncomplexed FKBP-12 from solution n.m.r. studies (Michnick *et al.*, 1991). Model building of FKBP-12 proceeded smoothly, but bound FK506 was not fit until electron density maps at higher resolution showed an unambiguous conformation for the entire molecule. The m.i.r. map was computed from experimental phases alone, no density modification procedures were employed.

(e) *Refinement of FKBP-12–FK506*

Model refinement was started at 3·0 Å, the resolution of the m.i.r. analysis and a low resolution cutoff of 10 Å was used throughout. Simulated annealing refinement, using the program X-PLOR with established protocols (Brünger *et al.*, 1990), was alternated with manual adjustments with respect to the m.i.r. electron density map. The initial model *R*-factor of 0·48 was rapidly reduced to 0·25 at 3·0 Å resolution while maintaining reasonable stereochemistry. Further rounds of simulated annealing refinement at 3·0 and 2·6 Å resolution were followed by manual adjustments with respect to $2F_o - F_c$ maps. Bound FK506 was initially fit at 2·6 Å resolution, but was first included in structure factor calculations and refined starting at 2·2 Å, where its conformation was unambiguous. Successive refinements extending the resolution from 2·0 to 1·7 Å converged quickly using least-squares minimization by the conjugate gradients method; simulated annealing refinements at high resolution resulted in an equivalent model structure.

Difference electron density maps following refinements revealed 134 ordered water molecules. Water sites with electron density greater than 4σ in $F_o - F_c$ maps were added to the model and those less than 1σ in the $2F_o - F_c$ map following refinement were rejected. The final solvent list was ordered on electron density. The thermal parameters of all model atoms and the occupancies of water molecules were refined without constraints, although occupancies were adjusted between cycles to lie between 0 and 1. The stereochemical terms used for FK506 refinement were restricted to those involving bonds, angles, planar groups and chiral centers. No planarity restraints were placed on the amide group of FK506. The overall *R*-factor for 17,038 reflections with $F/\sigma(F) > 3·0$ out of 18,605 total reflections at 10 to 1·4 Å resolution is 0·175. Results of the refinement are given in Table 1.

(f) *Molecular replacement solution of FKBP-12–rapamycin*

Molecular replacement calculations were carried out using the program MERLOT (Fitzgerald, 1988) with 25 to 4·0 Å resolution data. FKBP-12 from the complex with FK506, after refinement at 10 to 1·7 Å resolution (Van Duyne *et al.*, 1991*a*,*b*), was used as a search model and all atoms were included. The highest peak in the fast rotation function was 5 times the r.m.s. value and translation function calculations led to an unambiguous placement of the oriented model. Rigid body refinement of the model with X-PLOR gave an *R*-factor of 0·39 for 25 to 3·0 Å data.

(g) *Refinement of FKBP-12–rapamycin*

The FKBP-12–rapamycin complex was refined by conjugate gradient least squares minimization at 3·0, 2·6, 2·2, 2·0, 1·8 and 1·7 Å resolutions, in each case followed by calculation of $2F_o - F_c$ and/or $F_o - F_c$ maps for adjustments of the model and location of solvent atoms. Only one region, residues 31 to 34, required extensive adjustments of the main-chain atoms. Bound rapamycin was fitted to the $2F_o - F_c$ map following refinement at 2·6 Å and required only minor adjustments thereafter. The final stages of refinement proceeded as described for the FK506 complex and a corresponding set of stereochemical restraints was applied to refinement of bound rapamycin. The selection criteria and final numbering method for solvent molecules were also as described for the FK506 complex. Alternate conformations were identified and modeled for residues I90 and V98. The overall *R*-factor for 10,633 reflections with $F/\sigma(F) > 3·0$ out of 12,991 total reflections at 10 to 1·7 Å resolution is 0·154. Results of the refinement are given in Table 1.

(h) *Computational methods and conventions*

Model building and model adjustments following refinement were carried out with the programs FREIBAU (Karplus *et al.*, 1991) and CHAIN (Sack, 1988) on Hewlett Packard and Silicon Graphics workstations. Crystallographic refinements were done on a Convex C210 computer using the program X-PLOR (Brünger *et al.*, 1987). Secondary structure definitions follow those of Kabsch & Sander (1983) for helices and sheets and of Venkatachalam (1968) for β-turns. Surface areas were

calculated with the program QUANTA (Polygen Corporation, 1990). Other calculations were performed with locally written programs.

(i) *Data deposition*

Co-ordinates for all atoms in the final models of FKBP-12–FK506 and FKBP-12 rapamycin have been deposited with the Protein Data Bank. The accession number for the FKBP-12–FK506 complex is 1FKF; the accession number for the FKBP-12–rapamycin complex is not yet available.

3. Results and Discussion

(a) *Accuracy and comparison of the models*

Most main-chain and side-chain atoms and all ligand atoms in both the FK506 and the rapamycin complexes are represented by strong electron density, allowing unambiguous assignment of conformations. We estimate the level of accuracy of the structures to be approximately 0·15 Å, based on the value of the *R*-factors as a function of resolution as shown in Figure 3. The *R*-factor distributions for both structures lie between the theoretical curves corresponding to mean co-ordinate errors of 0·13 and 0·18 Å (Luzzati, 1952). At low resolution, an incomplete description of the solvent component of the crystal limits the agreement and at high resolution, the accuracy of the data plays a limiting role. As expected, the agreement of model and data is slightly better for the FK506 complex than for the rapamycin complex at a given resolution. Based on the average thermal parameters shown in Table 1, the error estimate of 0·15 Å should be representative of most main-chain atoms and particularly the ligand atoms. The average main-chain thermal parameters for both structures are shown graphically in Figure 4. The main-chain regions with higher than average thermal parameters and less well defined conformations in electron density maps are Gly19 in the FK506 complex and residues 31 to 34 and 41 to 44 in the rapamycin complex.

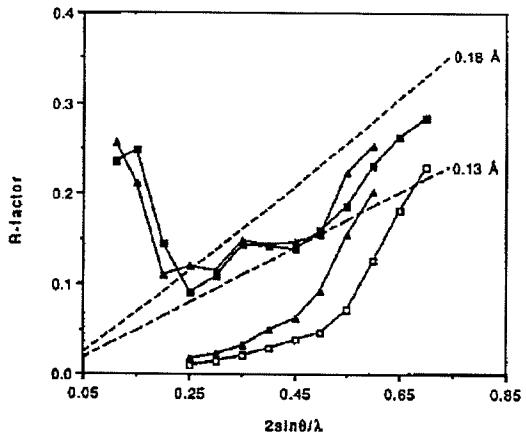

Figure 3. Luzzati plot for FKBP-12 FK506 (squares) and FKBP-12–rapamycin (triangles). The upper curves are *R*-factor *versus* resolution and the lower curves are R_{int} *versus* resolution, where $R_{int} = 2\Sigma(F_1 - F_2)/\Sigma(F_1 + F_2)$, and F_1, F_2 are the observed structure factor amplitudes of Friedel pairs for a given reflection. R_{int} gives an upper limit estimate of the level of error in the data.

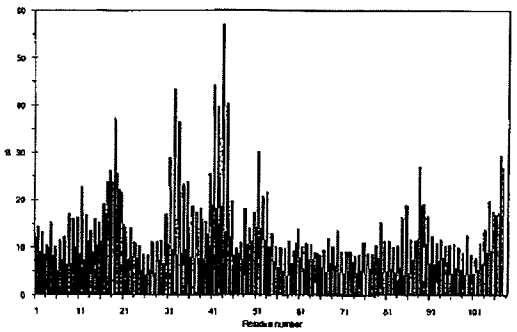

Figure 4. Average main-chain thermal parameters for FKBP-12–FK506 (dark) and FKBP-12–rapamycin (light).

Overall, the protein conformations in the two complexes are nearly identical. Figure 5 shows the average deviations for both main-chain and side-chain atoms for each residue, based on a superposition of main-chain atoms. The largest difference occurs for residues 31 to 34, the turn between strands 4 and 5 of the β sheet. Residues 18 to 20 and 50 to 51 also differ in the two complexes, with average main-chain separations of more than 1 Å. Figures 4 and 5 show a high degree of correlation, regions with higher thermal parameters, suggesting greater mobility, are those with the largest discrepancy between the two complexes. A least-squares superposition of the two protein structures using all main-chain atoms except residues 31 to 34 gives r.m.s. deviations of 0·48 Å for those main-chain atoms and 1·64 Å for all atoms. A least-squares fit using only the main-chain atoms of the 29 most buried residues (with less than 20 Å^2 solvent-accessible surface area) gives an r.m.s. deviation of 0·37 Å

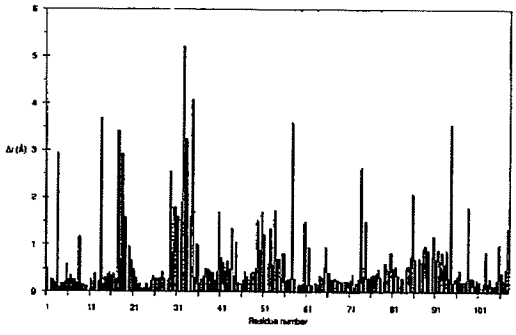

Figure 5. Average main-chain (dark) and side-chain (light) deviations for FKBP-12–rapamycin superimposed onto FKBP-12–FK506 by a least-squares fit of the main-chain atoms for residues 1 to 30 and 35 to 107.

Table 4
Intermolecular contacts

Type	Symmetry operation	Number of contacts	Residues involved	Hydrogen bonds	Bridging water molecules	Surface area buried (Å²)
FKBP-12–FK506: total surface area buried by crystal contacts = 3191 Å² (53%)						
1	$y, x, 1-z$	111	53, 55–57, 79, 80, 82–89, 91, 93, FK506	12	5	836
2	$1-y, 1-x, 1-z$	29	36, 42, 87, 88, 90, FK506	0	4	537
3	$-1/2+y, 1/2-x, 1/2+z$	28	3, 31, 32, 92, 94, 96	0	7	370
3′	$1/2-y, 1/2+x, -1/2+z$	28	8–11, 13, 69, 102, 104	0	7	389
4	$-x, 1-y, z$	25	5–7, 73	4	2	234
5	$1-x, 1-y, z$	10	21, 49, 52, FK506	2	2	229
6	$-1/2+y, 1/2-x, -1/2+z$	10	12, 15, 65	0	2	169
6′	$1/2-y, 1/2+x, 1/2+z$	10	32–34	0	2	180
7	$1/2-x, 1/2+y, 1/2-z$	2	43	0	2	173
7′	$1/2-x, -1/2+y, 1/2-z$	2	64, 65	0	2	157
FKBP-12–rapamycin: total surface area buried by crystal contacts = 1983 Å² (32%)						
1	$-x, 1/2+y, 1/2-z$	39	42, 44, 47, 87–90, rapamycin	2	1	596
1′	$-x, -1/2+y, 1/2-z$	39	5–9, 27, 29, 31, 32, 71, 73, 98, 100	2	1	538
2	$1/2-x, -y, -1/2+z$	22	12, 15, 65		3	252
2′	$1/2-x, -y, 1/2+z$	22	84, 92–94		3	254
5	$-1/2-x, -y, -1/2+z$	7	11–13		1	67
5′	$-1/2-x, -y, 1/2+z$	7	43		1	87
4	$1/2+x, 1/2-y, -z$	2	53		0	90
4′	$-1/2+x, 1/2-y, -z$	2	107		0	83

The number of contacts given is the number of atom–atom distances of less than 4 Å between listed residues from the complex in the reference asymmetric unit and residues from a complex generated by the given symmetry operation. Except for 2-fold symmetry operations, contacts are listed in pairs with the partner denoted by a prime. Thus the FK506 complex makes contact with 10 neighboring molecules, for example in interaction type 7 residue 43 contacts residues 64 and 65 on a neighboring complex, and residues 64 and 65 contact residue 43 on a neighboring complex. Hydrogen bonds have donor–acceptor distances <3·3 Å for this Table. Bridging water molecules are those water molecules with at least 1 hydrogen bond to the reference complex and 1 to a neighboring complex.

for those atoms, 0·59 Å for all atoms in the 29 residues, and 1·66 Å for all protein atoms. Thus, the agreement between the most well determined atoms in the two protein structures is two to three times their estimated error. This agreement is similar to that found in other analyses of proteins in different space groups and reflects the plasticity of protein core structures (Wlodawer *et al.*, 1987).

(b) *Intermolecular contacts*

The interactions between protein molecules in the crystal that lead to the long-range order required for a high resolution structure analysis can ironically diminish the relevance of some structural details. Therefore, it is important at the outset to discuss the locations of crystal contacts and any limitations they may place on conclusions drawn from these structural results. A summary of the intermolecular contacts for the FK506 and rapamycin complexes is given in Table 4. Crystals of the FK506 complex are 32% solvent by volume, have lower average thermal parameters, and each complex makes 255 total contacts of less than 4 Å with neighboring molecules. The rapamycin crystal structure is 48% solvent, has higher thermal parameters, and as expected, makes many fewer contacts, 142. Only 18 of the contacts in the FK506 complex and four in the rapamycin complex are intermolecular hydrogen bonds with good geometry. This major difference in crystalline environments is certainly responsible for some of the deviations between the two complexes. In general the residues that differ the most as shown in Figure 5 are in regions that are involved in either a large number of contacts or very different numbers of contacts in the two complexes.

The most conspicuous regions of the complexes which are involved in crystal contacts are the ligands themselves. FK506 makes a total of 29 and rapamycin 22 intermolecular van der Waal's contacts. All of the exposed regions of bound FK506 have atoms involved in contacts, with symmetry-related FK506 molecules (the allyl group at C21 is close to a site of crystallographic 222 symmetry) and with residues 82 to 90 of a neighboring FKBP-12. One of these contacts is an intermolecular hydrogen bond involving the cyclohexyl C32-hydroxyl of FK506. The rapamycin contacts involve most of the exposed regions of the ligand, including the C15 to C28 loop but not the cyclohexyl group.

(c) *Solvent structure*

A total of 134 water molecules for the FK506 complex and 133 water molecules for the rapamycin complex were included in the refined models. Since the space groups, and thus the packing arrangements, of the protein–ligand complexes differ substantially between the FKBP-12–FK506 and FKBP-12–rapamycin crystal structures, it is possible to differentiate between two kinds of bound water molecules: those that are common to the two

Table 5

Water molecules found in both the FKBP-12–FK506 and FKBP-12–rapamycin complexes and the most tightly bound water molecules unique to each of the complexes

FKBP-12–FK506 water no.†	$2F_o-F_c$ density (e/Å^3)	FKBP-12–rapamycin water no.†	$2F_o-F_c$ density (e/Å^2)	Pair distance (Å)	Hydrogen bonds to protein
1	4·3	1	2·5	0·4	G93, P92, A95
2	4·2	2	2·4	0·3	Y82, A95
4	3·5	14	1·7	1·0	M49, E54, E60
5	3·4	15	1·6	0·5	S67, Q70
6	3·1	42	1·1	1·4	T85
7	3·0	4	2·1	0·3	E5, K73, T75
8	2·9	3	2·3	0·4	G10
9	2·7	50	1·0	1·2	K35
11	2·5	85	0·9	0·5	K47
13	2·4	113	0·8	1·1	E31, T96
14	2·3	10	1·8	1·0	H94, T96
14′	2·3	49	1·1	0·5	V68
15	2·2	17′	1·5	1·2	T75
18	2·0	69	1·0	0·8	G1, D79
20	2·0	46	1·1	1·1	V2, Q65
22	2·0	52	1·0	0·4	G10
24	2·0	6	2·0	0·7	T75
25	1·9	29	1·3	0·7	V4
27	1·9	44	1·1	0·7	T6
28	1·9	61	1·0	1·3	P9
29′	1·9	7	1·8	1·4	P93
30	1·8	39	1·2	0·5	L106
31	1·8	16	1·6	0·7	P16, A64
33	1·7	9	1·8	1·1	Q65, Q70
35	1·7	5	2·0	0·6	V2
37′	1·6	21	1·4	1·3	H87
39	1·6	41	1·2	0·6	T6
40	1·6	68	1·0	0·4	R42, K44
52	1·4	38	1·2	0·7	E60
55	1·4	43	1·1	0·7	F15
68	1·3	34	1·3	1·0	R71
73	1·3	60	1·0	0·6	V4
80	1·2	128	0·7	0·2	R71
86	1·2	124	0·7	0·5	E54
88′	1·2	22	1·4	0·7	T96
96	1·1	19	1·4	0·9	Ligand C10-O
100	1·1	40	1·2	1·3	T27
102	1·1	57	1·0	0·5	F15, Q20
110	1·1	110	0·8	1·0	I90
123	1·0	117	0·8	1·0	K52
127	0·9	58	1·0	1·5	G69, E102
130′	0·9	126	0·7	0·6	E61
131	0·9	64	1·0	1·2	D79
3	3·8				T85‡
10	2·5				V55‡
12	2·4				Q53, E60‡
16	2·1				G89‖
17	2·0				A81‖
19	2·0				L30‡
21	2·0				FK506 C13-O, C15-O§
23	2·0				FK506 C22-O§
		8	1·8		T27, R40‡
		11	1·8		R40, D100‡
		12	1·7		E61§
		13	1·7		R57, A81§
		18	1·5		D37, rapamycin C16-O¶
		20	1·4		E54‡
		23	1·4		E31§
		24	1·3		A84§
		25	1·3		T6§

† Primes on water numbers indicate a position related by symmetry to the one in the asymmetric unit.
‡ Different side-chain conformation in the other complex.
§ Occupied by crystal packing interactions in the other complex.
‖ Requires crystal packing interactions.
¶ Disallowed by presence of C43 in FK506.

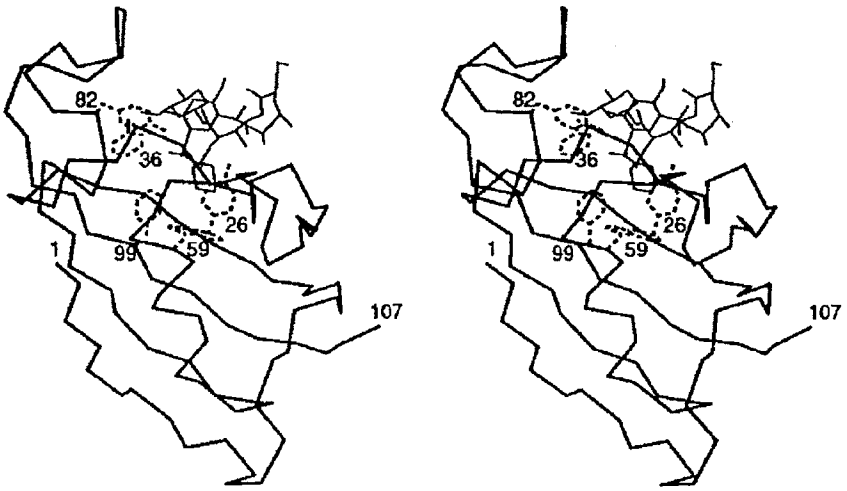

Figure 6. An α-carbon atom tracing of FKBP-12 (dark) showing bound FK506 (light) and the completely conserved aromatic residues (broken line) in the ligand binding pocket.

structures and candidates for structural components of the protein, and those that are dependent on the locations of neighboring protein molecules in the crystal. Of the 134 water molecules in the FK506 complex, 42 have mates in the rapamycin complex that are within 1·5 Å and that make a similar set of hydrogen bonds with the protein or ligand (Table 5). We chose a generous 1·5 Å cutoff for comparing water molecules between the two structures because of the large (0·49 Å) r.m.s. deviation between them and the observation that several water pairs differing by 1 to 1·5 Å maintained the same hydrogen bonding environments usually including side-chains that adopt slightly different conformations in the two complexes. Most of the common water molecules have high electron density and are tightly bound to the protein, but the entire range of refined solvent is represented in the list. As indicated in Table 5, all of the tightly bound water molecules that are not common to the two complexes are readily explained.

(d) *Structure of the protein*

The overall protein structure is a five-stranded antiparallel β-sheet wrapping with a right-handed twist around a short α-helix, shown schematically in Figure 2(b). A stereo drawing of the protein–ligand complex is shown in Figure 6. The protein core is composed exclusively of hydrophobic residues, many of them highly conserved among FKBPs found in different organisms (see below). Although FKBP-12 is a relatively small protein, most secondary structural elements are represented, β-sheet, α-helix, 3_{10}-helix, and an assortment of turns. The topology of the β-sheet is +3, +1, −3, +1 which, as shown in Figure 2(b), requires a topological crossing of loops, a folding element rarely observed in antiparallel sheets (Richardson, 1977). Such loop crossings have the interesting feature of resulting in distinct topologies, depending on which of the two crossing chains is on the top. One explanation for the lack of loop crossings has focused on the difficulty of satisfying hydrogen bonds when burying a non-regular main-chain protein segment in a hydrophobic protein interior (Ptitsyn & Finkelstein, 1980).

The physical loop crossing in the FKBP-12 structure, shown in Figure 7(a), involves a turn and a bend: at residues S67 to Q70 between the α-helix and strand two of the β-sheet and residues D11 to T14 that follow the first strand of the sheet. Residues 67 to 70 form a type II turn that is largely buried and forms the inner loop, with 96 $Å^2$ of solvent-accessible surface area. The bend involving residues 11 to 14 has no internal main-chain hydrogen bonds, but results in a roughly 90° change in direction in the chain between residues 10 and 15. This bend is largely exposed and forms the outer loop, with 389 $Å^2$ of surface-accessible; in fact, there are no buried side-chains in the P9-F15 segment. The two loops interact through two main-chain to main-chain hydrogen bonds, D11-N to V68-O and T14-O to V68-N, which serve to partially satisfy the hydrogen bonding requirements of the buried inner loop. The 11 to 14 turn is further stabilized by hydrogen bonds from both T14-O^{γ} and T14-N to the D11-carboxylate.

Other FKBPs may have additional or alternative methods of stabilizing the loop crossing region. Human FKBP-13, for example, contains G12C and S67C changes leading to a possible 12–67 disulfide bond (Jin *et al.*, 1991). With reference to the FKBP-12–ligand crystal structure complexes, disulfide formation at these locations would require an alternate conformation for the 11 to 14 loop.

A conformational change in FKBP-13 is also required to accommodate an R13P change, since R13 has $\phi = -140°$ in FKBP-12.

Residues K17 to Q20 form a type II turn in both complexes between the loop crossing region and the fourth strand of the β-sheet, although the loops are shifted with respect to one another by about 1 Å (Table 4). In neither case are these residues involved in intermolecular contacts, nor are they involved in or near the ligand binding site. G19 has the least well-defined main-chain conformation in the FK506 complex and in both complexes the 17 to 20 region has generally high thermal parameters, indicating a high degree of mobility. The turn involving residues E31 to K34 between strands 4 and 5 of the β-sheet also differs in the two complexes, but to a greater degree. The FK506 complex contains a type I turn, whereas the rapamycin complex contains a type II turn. These residues are not involved in ligand binding, but in both complexes they are involved in

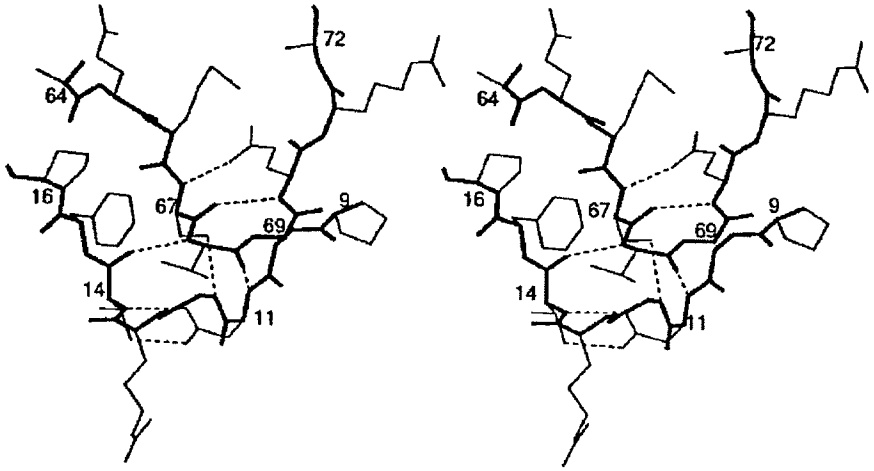

(a)

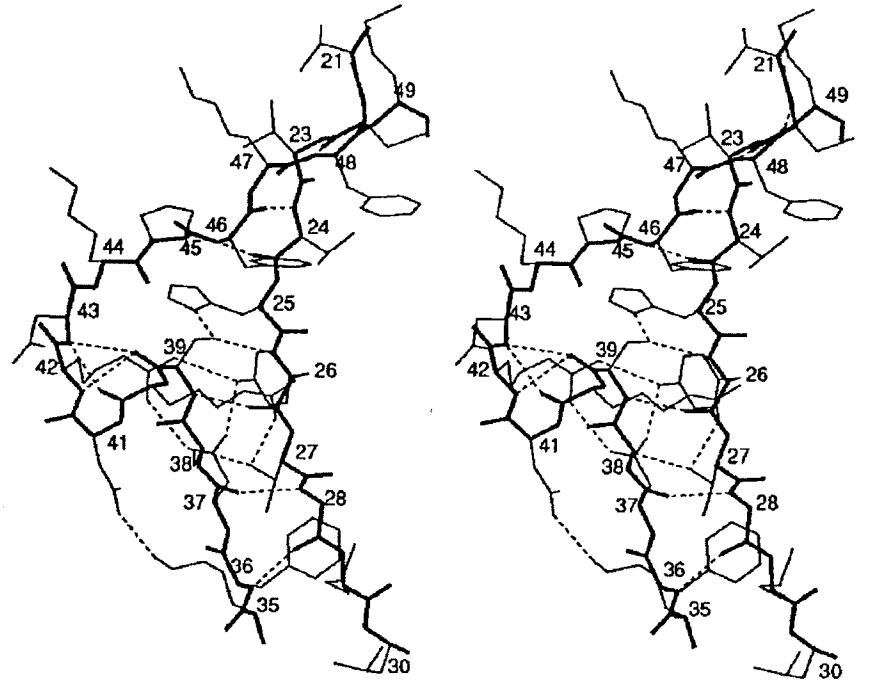

(b)

Fig. 7.

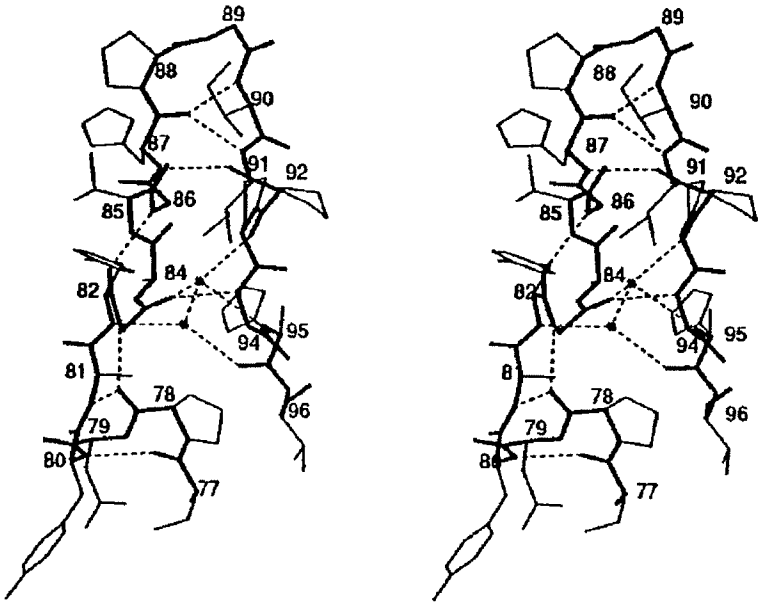

Figure 7. (a) The loop crossing region in FKBP-12–FK506 showing hydrogen bonding interactions. Residues 9 to 16 and 64 to 72 are shown. (b) Strands 4 and 5 of the β-sheet in FKBP-12–FK506 showing the bulge, the Y26-D37-R42 triad, and the 40-42 helix. Residues 21 to 30 and 35 to 49 are shown. (c) The 77 to 96 loop in FKBP-12–FK506 showing kcal turns, including the 78 to 80 3_{10}-helix and the 2 most tightly bound, buried water molecules. Main-chain and ligand bonds are drawn with bold, side-chains with light, and hydrogen bonds with broken lines.

intermolecular contacts (Table 4): 17 contacts involving main-chain and side-chain atoms in the FK506 complex and seven contacts involving only E31 and D32 side-chain atoms in the rapamycin complex. We attribute this largest difference between protein structures in the two complexes to the different crystalline environments. Interestingly, the solution structure of uncomplexed FKBP-12 (Michnick *et al.*, 1991) contains the type II turn, in agreement with the turn found in the less restricted rapamycin complex.

The fifth strand of the β-sheet is split, with a seven-residue disruption of the regular secondary structure that forms a large bulge in the strand, as shown in Figure 7(b). This bulge may serve as a convenient insertion point for recognition sequences that would not require major changes in protein structure (see Fig. 12). Human FKBP-30, for example, contains a possible nuclear translocation sequence in this region (Galat *et al.*, 1992). In the FKBP-12–FK506 and rapamycin complexes the bulge plays a role in organizing the ligand binding pocket, with R42 involved in an Arg-Asp-Tyr triad. The bulge contains a five-residue turn with a hydrogen bond between S39-O and K44-N and a short, irregular 3_{10} helix involving residues 40 to 42. The average main-chain difference between the two complexes is about 0·5 Å in this region. The two pieces of the fifth strand of the β-sheet on either side of the bulge are each four residues long, making a total of eight main-chain–main-chain hydrogen bonds. In both complexes the strand-bulge-strand assembly is further stabilized by cross-strand hydrogen bonds involving side-chains (Y26-N to S39-O$^{\gamma}$ and T27-O$^{\gamma}$ to S38-O$^{\gamma}$) and three salt bridges involving basic side-chains found in the bulge (K35–D41, R40–D102 and R42–D37). Amino acids T27, S38 and S39 are strongly conserved among FKBPs, suggesting that these stabilizing interactions are significant.

The M49 to V55 loop connecting the fifth strand of the sheet and the α-helix (Fig. 6) contains a type II turn at residues M49 to K52 that is the third region where the main-chain atoms in the FK506 and rapamycin complexes differ by more than 0·5 Å. The residues that follow the turn and lead into the N terminus of the helix play an important role in ligand binding, making two hydrogen bonds to FK506 and three to rapamycin as well as providing an important component of the hydrophobic binding pocket with side-chains from V55 and I56. In the FKBP-12–rapamycin complex there is a hydrogen bond, G19-N to L50-O, from the main-chain of an adjacent loop. This interaction has the effect of extending the number of hydrogen bonds in the second segment of strand 5 of the sheet. The only short crystal contacts in these loops occur in the 49 to 52 region of the FK506 complex (4 contacts). Hydrogen bonds from M49-N and G51-N to E54-O$^{\epsilon}$ and E60-O$^{\epsilon}$, respectively, and a weak

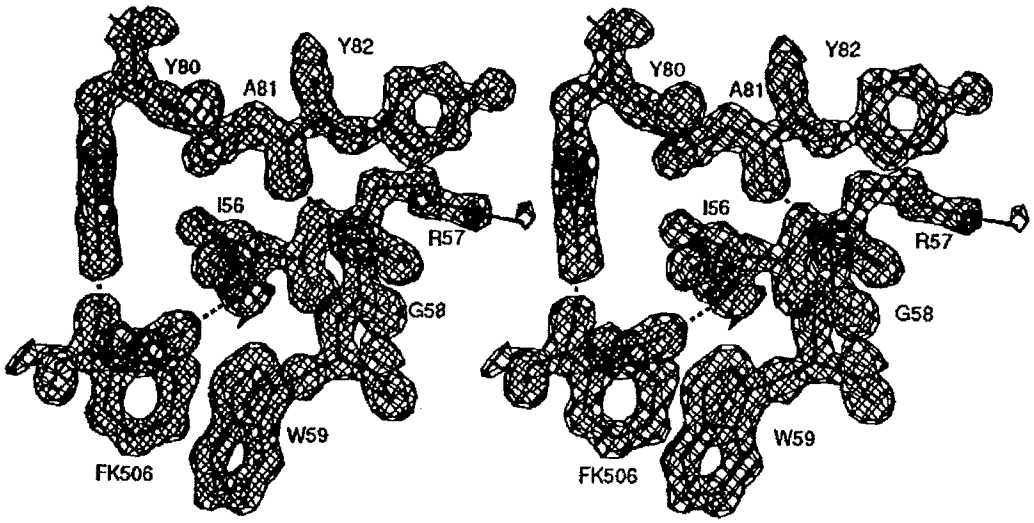

Figure 8. Electron density showing the 56 to 59 and 80 to 82 regions, the C1 to C9 region of bound FK506, and the 2 hydrogen bonds between the 77 to 96 loop and the rest of the complex. The electron density is from the final $2F_o - F_c$ map for the FKBP-12–FK506 structure and is contoured at 1·5σ, or 15% of the maximum value.

hydrogen bond between M49-O and E54-N serve to immobilize this important region.

The α-helix in FKBP-12 (Fig. 6) buries residues G58, W59, G62 and V63 in the core of the protein and leaves R57, E60, E61, A64 and Q65 exposed, with a salt bridge between R57 and E61. The N terminus of the helix is stabilized by G58-N to Y80-O and W59-N to I56-O hydrogen bonds in both complexes and in the rapamycin complex by a bound water molecule near R57-N. The C terminus of the helix makes a V63-O to M66-N hydrogen bond and binds water molecules common to both complexes at A64 and Q65 main-chain carbonyl groups. In addition, a surface phenylalanine side-chain, F15, is oriented with an aromatic hydrogen atom directed along the axis of the helix at the C terminus, approximately 3 Å from the A64 carbonyl group in both complexes.

The largest loop in the FKBP-12 structure is 20 residues long, from S77 to T96 between strands 2 and 3 of the sheet (see Fig. 7(c)). The main-chain is tightly associated across the loop by hydrogen bonds and bridging water molecules. A series of local turns produces an overall loop of loops configuration forming a flap that folds over the protein and the ligand binding site. Residues P78 to G83 form a six-residue turn containing a short 3_{10}-helical segment at residues P78 to Y80, followed by a five-residue turn starting at Y82 that uses two hydrogen bonds. Residues H87 to I91 form a two-hydrogen-bonded turn that results in the 180° change in direction of the overall loop, followed by a type II turn at P92 to A95. The two most tightly bound water molecules (see Table 5) in both complexes bridge the loop between G83-O and P92-O, between Y82-N and A95-O (see Fig. 7(c)). Both water molecules are located between the flap and protein core and are completely buried. A strong hydrogen bond between G83-O and H94-N also bridges the loop.

Two hydrogen bonds are formed between the 20-residue flap and the rest of the complex. The first is the Y80-O to G58-N interaction with the N terminus of the α-helix. The second is between Y82-OH and the amide carbonyl group of the bound ligand. Located between these two amino acids, A81 is the sole non-glycine residue with ϕ, ψ angles outside the low energy regions of a Ramachandran plot: (−142°, −118°) for FKBP-12–FK506 and (−132°, −118°) for FKBP-12–rapamycin, conformations where C^β eclipses N. A81 is highly conserved with only glycine substitutions occurring in other FKBP sequences and is well-defined in the electron density map (Fig. 8). The 77 to 96 loop adopts a single, well-defined conformation in these ligand complex crystal structures, but in solution and in the absence of ligand, this loop has been shown to be quite flexible, able to adopt an ensemble of low energy configurations (Michnick *et al.*, 1991). A portion of the electron density for this region of the FKBP-12–FK506 structure is shown in Figure 8.

(c) *Ligand binding*

FK506 and rapamycin bind in a hydrophobic cavity between the α-helix and the interior wall of the β-sheet that is lined with a number of highly conserved, aromatic residues (Fig. 6). The cavity is flanked by the 39 to 45 bulge in the fifth strand of the sheet, the 49 to 56 segment leading into the helix, and the 77 to 96 loop. The pipecolinyl ring (C2 to N7) makes the deepest penetration into the protein where it is surrounded by the aromatic rings of

Table 6
Protein–ligand interactions

	Contacts less than 4 Å		Hydrogen bonds and C–H···O interactions				
Ligand region	Protein residues	No. contacts	Donor	Acceptor	H···O (Å)	X–H···O (°)	H···O–X (°)
FKBP–FK506							
C1	V55, I56, Y82	11	I56-N	C1-carbonyl	1·92	150	148
C2-N7	Y26, F46, V55, W59, Y82	21	Y82-OH	C8-carbonyl	1·86	151	131
C8-C9	Y26, F36, D37, Y82, F99	13	C10-hydroxyl	D37-O$^{\delta}$	1·74	175	118
C10-C14	Y26, D37, Y82, H87, I91	12	C24-hydroxyl	E54-O	1·88	138	137
C15-C17	Y26, D37, R42, F46	9	Y26-CεH	C9-carbonyl	2·72	126	136
C24-C26	F46, E54	7	F36-CεH	C9-carbonyl	2·43	156	103
C27-C34	I56, A81, Y82	5	F99 CεH	C9-carbonyl	2·52	149	121
FKBP–rapamycin							
C1	V55, I56, Y82	9	I56-N	C1-carbonyl	2·11	155	152
C2-N7	Y26, F46, V55, W59, Y82	23	Y82-OH	C8-carbonyl	1·88	150	132
C8-C9	Y26, F36, D37, Y82, F99	16	C10-hydroxyl	D37-O$^{\delta}$	1·78	177	105
C10-C14	Y26, D37, Y82, H87, I90	10	C28-hydroxyl	E54-O	1·92	157	119
C44	F46	1	C40-hydroxyl	Q53-O	1·81	162	142
C46	E54	1	Y26-CεH	C9-carbonyl	2·68	127	142
C28-C32	D37, F46, E54, V55	12	F36-CεH	C9-carbonyl	2·21	161	105
C35-C42	Q53, E54, V55, I56, Y82, H87	15	F99-CεH	C9-carbonyl	2·74	146	124

Y26, F46, W59 and F99. FK506 and rapamycin share a common binding domain composed of the C1 to C14 region, which includes the ester linkage, the pipecolinyl ring, the dicarbonyl and the hemiketal ring. The synthetic tight binder 506BD (Bierer *et al.*, 1990*b*) also contains this region. Most of the ligand–protein contacts involve these groups and are summarized in Table 6. The entire protein–ligand interface buries 450 Å^2 (47%) of the total FK506 solvent-accessible surface and 505 Å^2 (49%) of rapamycin with a total of four protein–ligand hydrogen bonds for FK506 and five for rapamycin. The exposed regions of the bound ligands include the C17 to C22 region in FK506 and the C14 to C23 region in rapamycin.

The atomic positions and interactions with FKBP-12 in the common binding domain are equivalent in the FK506 and rapamycin complexes. The r.m.s. deviation for these 21 atoms is 0·48 Å using a superposition of main-chain protein atoms, excluding residues 31 to 34. This r.m.s. deviation reduces to 0·1 Å if only the 21 atoms are superimposed. At one end of the common binding domain, the ester carbonyl group at C1 accepts a hydrogen bond with good geometry from 156-N at the N terminus of the helix. The pipecolinyl amide carbonyl group at C8 accepts an atypical hydrogen bond from Y82-OH that is nearly perpendicular to the plane of the carbonyl group, with a C9-C8-O···H torsion angle of −112° in the FK506 complex and −127° in the rapamycin complex. This hydrogen bond is one of two involving the 77 to 96 flap and may be partially responsible for the anomalous ϕ, ψ angles of A81. The amide group, which was not constrained to planarity in refinement, is perfectly planar, with a C2-N7-C8-C9 torsion angle of 180° in both complexes. Y82 is strictly conserved among known FKBP-12 sequences, indicating that this hydrogen bond may also be relevant to the natural function of FKBP-12. Figure 9 shows the protein–ligand interactions involving the 50 to 56 loop and the 77 to 96 flap for both the FK506 and rapamycin complexes.

The C9 carbonyl group is perpendicular to the plane of the amide group with an O-C8-C9-O torsion angle of −91° in FK506 and −90° in rapamycin. There are no hydrogen bonds to this carbonyl group, but three completely conserved aromatic side-chains, Y26, F36 and F99, have ε-hydrogen atoms directed toward the carbonyl oxygen atom and provide an unusual kind of carbonyl solvation involving aromatic C-H···O interactions. The geometries of these interactions are listed in Table 6. Taylor & Kennard (1982) found a large number of C-H···O interactions in a search of 113 organic crystal structures from the Cambridge Crystallographic Database and discovered that many of them have H···O distances 0·3 Å shorter than the sum of the van der Waal's radii for hydrogen (1·2 Å) and oxygen (1·5 Å). Thomas *et al.* (1982) found in a search of phenylalanine environments in 28 protein structures that aromatic C-H···O interactions were not only quite common, but that based on the spatial distribution of oxygen atoms, the interaction of an oxygen atom at the edge of the ring was more stable than at the top of the ring by roughly 1 kcal/mol (1 cal = 4·184 J). Theoretical calculations have supported the notion that C-H···O interactions are stabilizing (Wiberg *et al.*, 1991) and may contribute to the overall stability of folded proteins (Thomas *et al.*, 1982).

Using Taylor & Kennard's (1982) value of 2·7 Å for the H···O van der Waal's contact distance, the Y26 and F99 interactions in the FKBP-12–ligand complexes are not strikingly short, but the F36 interactions of 2·4 and 2·2 Å are significantly below this value. All six interactions involve the edges of the aromatic rings. Y26 and F99 are involved in

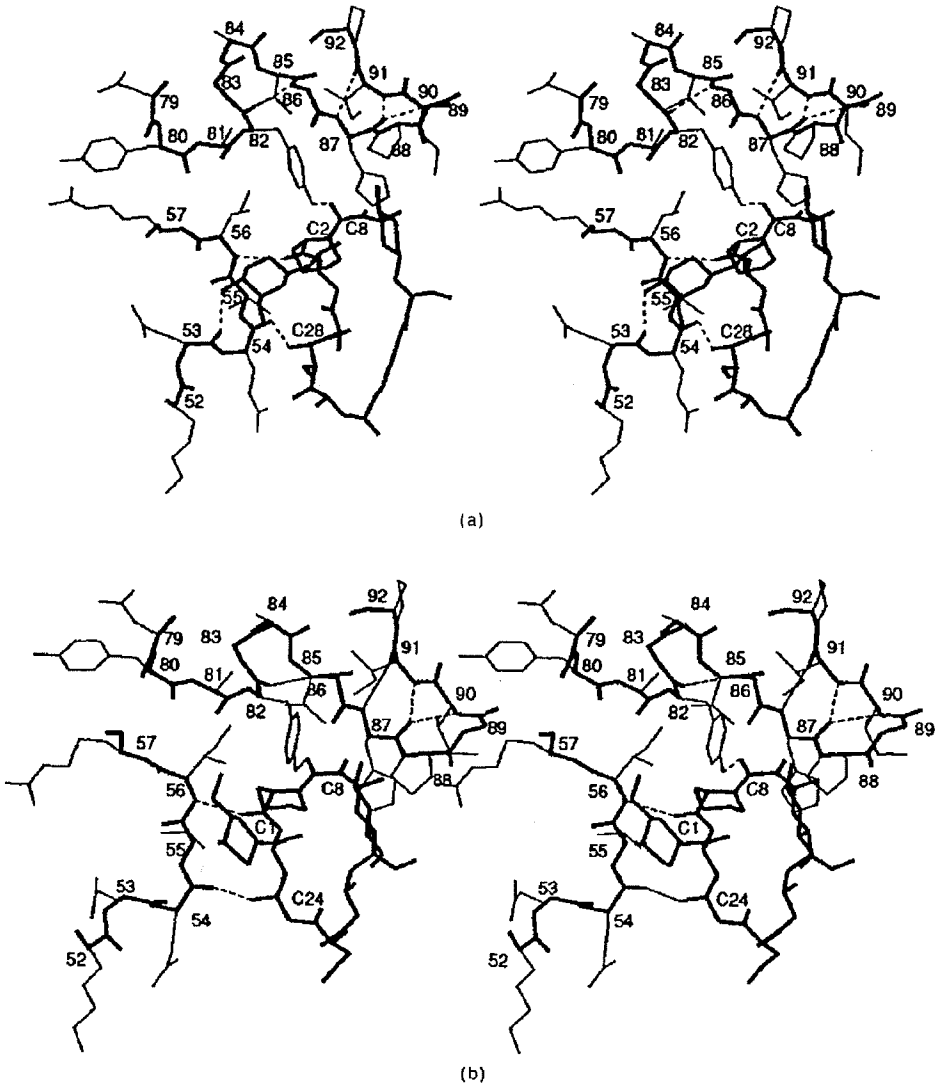

Figure 9. Protein–ligand interactions involving the 50 to 56 and 77 to 96 loops for (a) FKBP-12–FK506, and (b) FKBP-12–rapamycin. Ligand and main-chain protein bonds are drawn in bold, side-chains in light, and hydrogen bonds in broken lines.

other ligand contacts, but this is the only ligand interaction involving F36. From visual inspection of FKBP-12–ligand models, the role of F36 in maintaining the structural integrity of the hydrophobic protein core could be provided by other amino acids, suggesting that this short C-H···O interaction (and possibly the others) serves an important function in this protein.

At the end of the common binding domain, a cyclic hemiketal at C10, masking a third consecutive carbonyl group, makes a number of contacts with the protein and the C10-hydroxyl makes two hydrogen bonds: one to D37-O^{δ} and the other to a bound water molecule found in both complexes (Table 5). D37 also plays an important role in organization of the binding pocket, forming a salt bridge with R42 and a strong hydrogen bond with Y26-OH (see Fig. 7(b)). R42 also hydrogen bonds to Y26-OH, completing an Arg-Asp-Tyr triad (Horovitz *et al.*, 1990).

The FK506 C24 to C26 region and the rapamycin C28 to C34 region are chemically quite different, yet remarkably in the bound conformations they each provide a different hydroxyl group (C24-OH and C28-OH, respectively) that forms an equivalent hydrogen bond to E54-O. In contrast, the cyclohexyl region (C27 to C34 in FK506 and C35 to C42 in rapamycin) differs only by saturation of the

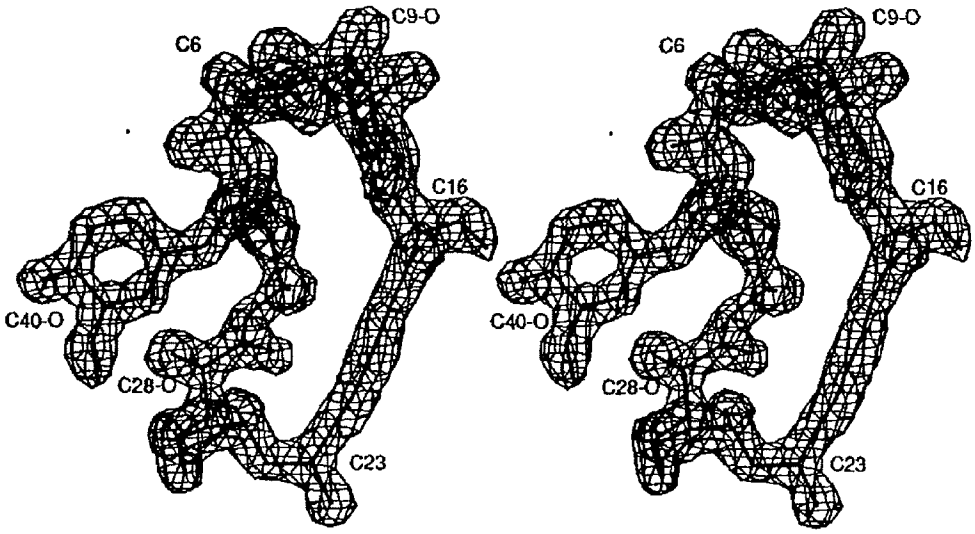

Figure 10. Electron density showing bound rapamycin. The electron density is from the final $2F_o - F_c$ map and is contoured at 2σ (26% of the maximum value).

C27–C28 bond, yet plays an entirely different role in the two complexes. The cyclohexyl ring is almost entirely exposed in the FK506 complex, making only three contacts from the C29 to C34 ring to FKBP-12 and an intermolecular hydrogen bond from the C32-hydroxyl group to a neighboring complex in the crystal. The same ring in rapamycin differs in orientation by a 180° rotation about the C37 to C40 vector and makes 11 contacts with the protein, including a hydrogen bond between the C40-hydroxyl group and Q53-O. This ring orientation and hydrogen bond formation is prevented in FK506 by the C27–C28 double bond.

At the outset of these studies, the bound *versus* unbound conformations of both FK506 and rapamycin were of great interest. The crystal structures of both compounds have been reported (Tanaka *et al.*, 1987; Swindells *et al.*, 1978), and they have very different conformations in the common binding domain. In crystalline FK506, the amide bond is *cis* and in rapamycin the amide bond is *trans*. In the structures of the complexes with FKBP-12 the amide bond is *trans* and the common 21 atom binding domains have identical conformations with an r.m.s. deviation of 0·1 Å, fitting independently of the protein. A comparison between bound and unbound FK506 shows a dramatic change in overall conformation, whereas bound and unbound rapamycin are nearly superimposable, with an r.m.s. difference of 0·49 Å. The preorganization of rapamycin for binding to FKBP-12, along with the extra hydrogen bond resulting from rotation of the cyclohexyl ring, may in part explain the twofold difference in binding constants for rapamycin (K_d = 0·2 nM) and FK506 (K_d = 0·4 nM) (Bierer *et al.*, 1990*a*,*b*). The electron density for rapamycin bound to FKBP-12 is shown in Figure 10.

(f) *Conserved amino acids*

The sequences of a number of FKBPs are listed in Figure 12 with probable roles for selected residues, many of which have already been discussed. A total of 13 residues in FKBP-12 are strictly conserved among the sequences shown and ten of these are involved in maintaining the hydrophobic core of the protein that forms the ligand binding pocket. The remaining three are glycine residues involved in turns. The first strand of the β-sheet is rather poorly conserved. This strand contributes no important side-chains to the hydrophobic core of the protein and may serve as the linker chain between domains in larger FKBPs.

Three of the highly conserved glycine residues not yet discussed play interesting roles in FKBP-12. G28 is a perfectly conserved residue that forms part of the β-sheet and consequently adopts ϕ, ψ angles readily accessible to other amino acids. A β-carbon atom in this position, however, would point directly into the binding pocket and occupy the space taken by the twisted carbonyl group at C9. Another strongly conserved glycine, G10, is located at the loop crossing region, where a side-chain would disrupt the observed loop–loop packing. G58 is in the helix and is almost perfectly conserved. A side-chain in this position would point into the hydrophobic core onto the I76 side-chain. The single G58A change in this position is correlated with an I76C change, allowing the alanine β-carbon atom the required space.

(g) *FKBP-12 as a rotamase*

Although the natural function of FKBP-12 is not yet known, its activity as a *cis–trans* peptidyl-prolyl isomerase (rotamase) has been established by two

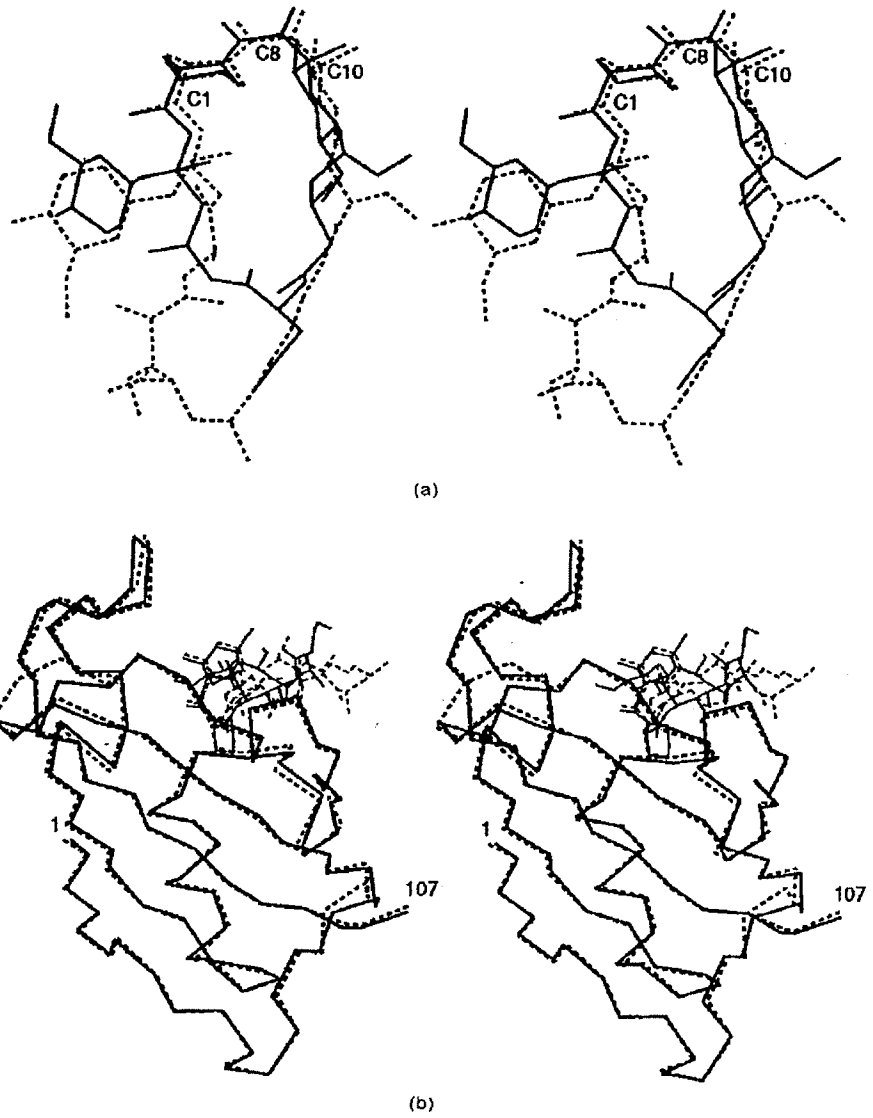

Figure 11. Superimpositions of (a) FK506 (continuous) and rapamycin (broken), and (b) FKBP-12–FK506 (continuous) and FKBP-12–rapamycin (broken) based on a fit of main-chain atoms from residues 1 to 30 and 35 to 107.

groups (Siekierka *et al.*, 1989; Harding *et al.*, 1989). As discussed earlier, this rotamase activity appears to be unrelated to the role of FK506 and rapamycin in immunosuppression (Schreiber, 1991). Nevertheless, the FKBP-12–FK506 and FKBP-12–rapamycin crystal structures represented the first high resolution models of a rotamase and may shed light on the mechanism of enzymatic proline isomerization. Two subsequent reports (Ke *et al.*, 1991; Kallen *et al.*, 1991) revealed high resolution X-ray structures of cyclophilin A, the archetypal representative of the other rotamase family. Recently, steady state kinetic parameters $K_m = 0{\cdot}52$ mM and $k_{cat} = 344\ s^{-1}$ have been reported for bovine FKBP-12 with the substrate succinyl-Ala-Leu-*cis*-Pro-Phe-*p*-nitroanilide, with a catalytic efficiency of roughly 10^5 and a corresponding decrease in activation energy of approximately 6 kcal/mol for the isomerization reaction (Kofron *et al.*, 1991).

The active site of FKBP-12 is a hydrophobic cavity that is part of a larger cleft formed as a result of the 77 to 96 flap folding onto the ligand binding region. It appears that both *cis* and *trans* peptide substrates could be accommodated in this binding pocket, although details of the interactions that would be involved are not yet clear. Models of FK506 and rapamycin binding to FKBP-12 have focused on an analogy between the common binding

```
                          •        • •       •      •*•* •  •*  **•      •       •
hFKBP12                   GVQVETISPG DGRTFPKRGQ TCVVHYTGML EDGKKFDS.....SR DRN..KPFKFML
bFKBP12                   GVQVETISPG DGRTFPKRGQ TCVVHYTGML EDGKKFDS.....SR DRN..KPFKFVL
hFKBP13              TGAEGKRK LQIGVKKRVD HCPIKSRKGD VLHMHYTGKL EDGTEFDS.....SL PQN..QPFVFSL
bFKBP25      ..SEETLDEGPP KYTKSVLKKG DKTNFPKKGD VVHCWYTGTL QDGTVFDTNIQTSSK KKKNAKPLSFKV
NCFKBP            MTIPQLD GLQIEVQQEG QGTRETRRGD NVDVHYKGVL TSGKKFDA.....SY DRG..EPLNFTV
SCFKBP            MSEVIEG NVKIDRISPG DGATFPKTGD LVTIHYTGTL ENGQKFDS.....SV DRG..SPFQCNI
NMFKBP                  M GSLIIEDLQE SFGKEAVKGK EITVHYTGWL EDGTKFDS.....SL DRR..QPLTITL
Lpneumip       NKPGVVVLPS GLQYKVINAG NGVKPGKSD. TVTVEYTGRL IDGTVFDS.....TE KTG..KPATFQV
Paerumip       ARFGVRELTG GVLVSELRRG QGNGIGAAT. QVHVRYRGLL ADGQVFDQ.....SE SA...WFALD..
Chtchlmip      KAGVIELEPN KLHDRVVKEG TGRVLSGKP. TALLHYTGSF IDGKVFDS.....SE KNK..EPILLPL
Mustrans2      GVDISPKQDE GVLKVIKREG TGTETPMIGD RVFVHYTGWL LDGTKFDS.....SL DRK..DKFSFDL
                          1          11         21         31               41
Secondary structure        <--β1->              <---β4--->     <β5>                <β5>
Comments                                     c       aba d   c  aab      b       c

               •   ** ••       •  *     • •     •**  •     •••  •* *   •*
hFKBP12        GKQEVIRGWE EGVAQMSVGQ RAKLTISPDY AYGATGHPGI IPPHATLVFD VELLKLE
bFKBP12        GKQEVIRGWE EGVAQMSVGQ RAKLTISPDY AYGATGHPGI IPPNATLIFD VELLKLE
hFKBP13        GTGQVIKGWD QGLLGMCEGE KRKLVIPSEL GYGERGAPPK IPGGATLVFE VELLKIERRTEL
bFKBP25        GIGKVIRGWD EALLTMSKGE KARLEIEPEW AYGKKGQPDx ixqpnxLIFE VELVDID
NCFKBP         GQGQVIKGWD EGLLGMKIGE KRKLTIAPHL AYGNRAVGGI IPANSTLIFE TELVGIKGVQKGE
SCFKBP         GVGQVIKGWD VGIPKLSVGE KARLTIPGPY AYGPRGFPGL IPPNSTLVFD VELLKVN
NMFKBP         GVGQVIKGWD EGFGGMKEGG KRKLTIPSEM GYGATRRGGV IPPHATLIFE VELLKVYE
Lpneumip       S  QVIPGWT EALQLMPAGS TWEIYVPSGL AYGPRSVGGP IGPNETLIFK IHLISVKKSS
Paerumip          SVIEGWR TALRAMPVGA RWRVVIPSAQ AYGHEGAGDL IPPDAPLVFE IDLLGFR
Chtchlmip      T  KVIPGFS QGMQGMKEGE VRVLYIHPDL AYGTAGQ... LPPNSLLIFE VKLIEANDDNVSVTE
Mustrans2      GKGEVIKAWD IAVATMKVGE VCHITCKPEY AYGAAGSPPK IPPNATLVFE VELFEFKGEDLTEEEDGGIIRRI
               51         61         71         81         91         101
Sec str.             <--α -->        <β2-->                     <---  β3--->
Comments       c   aa da       d  b     d d     cac  c     a c  d a     d
```

Figure 12. A comparison of FKBP sequences. Residue numbering and secondary structure assignment are for human FKBP-12 complexed with FK506 or rapamycin. Lower case sequence assignments indicate uncertainty. *, Perfect conservation; ●, >70% identity. a, Involved in ligand binding pocket; b, involved in structurally important hydrogen bonds; c, adopts special torsion angles; d, required to maintain hydrophobic core. hFKBP, human; bFKBP, bovine; NC, *Neurospora*; SC, yeast; NM, *Neisseria*; Lpneumip, *Legionella* macrophage infectivity potentiator; Chtchlmip, *Chlamydia* MIP; Mustrans2, mouse transition protein 2 homolog. Sequence data from Galat *et al.*, (1992).

domains of the two ligands and that of a proposed peptide substrate, where the pipecolinyl ring serves as a proline analog, the twisted carbonyl group (C9) mimics the transition state of a peptide substrate undergoing isomerization about the amide bond, and the C10-hydroxyl group and hemiketal ring play the role of amide and side-chain of the preceding residue (Albers *et al.*, 1990). The protein–ligand interactions already discussed provide the framework to evaluate this immunosuppressant-peptide analogy and to begin the process of unraveling the catalytic mechanism of rotamase activity.

A particularly revealing aspect of ligand binding to FKBP-12 involves the hemiacetal ring. FKBP-12 exhibits a strong preference for leucine as the residue preceding proline in peptide substrates (Albers *et al.*, 1990). Indeed, inspection of this region of the protein–ligand interface shows that the side-chain of the residue preceding proline in a peptide substrate would have access to a hydrophobic pocket that is well-suited for a leucine residue. In FK506 and rapamycin the C11-methyl group is directed into this pocket, in general agreement with a peptide mimic model. Donald *et al.* (1991) have shown that chemical modification of the C10-hydroxyl to a nitrogen and subsequent attachment of peptide-like fragments leads to mostly non-binding substrates and conclude that a direct peptide analogy breaks down in this region. It is clear from the FKBP-12–ligand crystal structures that such substitutions could not be accommodated and that on the fringes of the common binding region, the model of FK506 and rapamycin as peptide mimics becomes a topological one, where the ligands mimic a peptide substrate in the interactions they make with protein and not by an atom-by-atom analogy. These results underscore both the importance of detailed structure analysis and the limitations of any single model in formulating a general picture of FKBP-12–substrate interactions.

Current models of catalytic mechanisms for both cyclophilin (Harrison & Stein, 1990) and FKBP-12 (Rosen *et al.*, 1990) involve stabilization of the amide carbonyl atom as it rotates about the C–N bond. Scheiner & Kern (1977) have shown that desolvation should increase the flexibility of amide bonds and Kofron *et al.* (1991) point out that a hydrophobic active site may be a contributing factor in stabilization of the twisted carbonyl group for this reason. The extremely hydrophobic binding pocket of FKBP-12 is certainly consistent with this idea. Calculations by Wiberg *et al.* (1991) support experimental data showing that environments with lower dielectric constants result in higher energies for dipolar species. Wiberg & Laidig (1987) find that the charge distribution in a twisted amide group relative to the planar species is virtually unchanged at the carbonyl oxygen atom, is reduced at the nitrogen atom, and is less dipolar along the C–N

bond, in contrast to the traditional view of amide resonance where the oxygen atom is expected to experience a decrease and the nitrogen atom an increase in electron density upon distortion. These calculations also support the notion of stabilization of a twisted amide group in the low dielectric, hydrophobic binding pocket relative to the higher dielectric aqueous solvent.

The dicarbonyl binding region of the FKBP-12–FK506 and rapamycin complexes presents an intriguing set of interactions with respect to the amide group in a hypothetical peptide substrate. The Y82-OH to C7-carbonyl hydrogen bond appears to stabilize a planar, *trans*-amide, and the novel C8-carbonyl binding pocket involving C-H···O interactions appears to stabilize the twisted amide group. The same Y82 interaction would presumably not exist in a *cis*-amide substrate, but the side-chains of D37 and/or Y26 are in positions that could interact with the peptide carbonyl group from the opposite direction. Y82 appears to be capable of substantial rotation about χ^1, providing a great deal of flexibility in adapting to the possible motions of the substrate during catalysis. For both FK506 and rapamycin, such a rotation would result in a better hydrogen bond, more nearly in the plane of the C8 carbonyl group. Alternatively, Y82 could form a hydrogen bond with the nitrogen lone pair or a twisted carbonyl group, a novel way of lowering the barrier to amide rotation. The relevance of these interactions and the roles of D37, Y26 and Y82 are now the subject of ongoing studies involving both mutagenesis and substrate analogs.

(h) *FKBP-12 as an immunophilin*

The enormous attention that FK506, rapamycin, and their binding proteins have received is due to their medicinal value in modulating the immune response and also to their value as probes into the complex signal processing machinery that translates an extracellular signal into a cellular response. By now, incontrovertible evidence has accumulated that implicates the *complex* of FKBP-12 with FK506 or of FKBP-12 with rapamycin rather than any of the single components as responsible for disruption of signal transduction pathways (Koltin *et al.*, 1991). A truly fascinating aspect of this activity, in view of the similarity between the two complexes, is the differing pathways affected by FKBP-12–FK506 *versus* FKBP-12–rapamycin. Ultimately, each of these complexes must interact with a third component, a "partner protein", that must recognize FK506 or rapamycin, but only as presented by FKBP-12.

Cyclosporin A, which is structurally unrelated to rapamycin or FK506, and which interacts with a distinct family of immunophilins, is nonetheless believed to have a similar *modus operandi* in that it exerts its effect only when complexed with a cyclophilin, e.g. cyclophilin A. Indeed, it was recently discovered that the complexes of FKBP-12–FK506 and cyclophilin A–cyclosporin A competitively bind to and modulate the enzymatic activity of a common target, the Ca^{2+}-calmodulin-dependent protein phosphatase calcineurin (protein phosphatase 2B; Liu *et al.*, 1991). The structures of FKBP-12–FK506 and FKBP-12–rapamycin will figure prominently in understanding the molecular basis of the interactions of immunophilin–drug complexes with calcineurin and other targets that might emerge.

The crystal structures of the FKBP-12–FK506 and FKBP-12–rapamycin complexes described have nearly identical protein components in the drug-binding regions, despite large numbers of intermolecular contacts in the crystal lattices. The differences between the complexes in this region would thus appear to arise from the ligands themselves, and not ligand binding-induced changes in protein structure. Superimpositions of the two ligands and of the two complexes are shown in Figure 11. It is remarkable that despite the very different chemical structures of the exposed portions of FK506 and rapamycin, they project in the same general direction. The C17 to C22 triene of rapamycin, the C21 allyl group of FK506, and the differing cyclohexyl conformations are the most conspicuous exposed features for the two bound ligands. We cannot, however, rule out the possibility that areas remote from the ligand binding pocket that differ in conformation for the two complexes are important recognition elements. The relationship between these structural features and the elicited biological response is now an area of intense, multidisciplinary research.

We thank the National Cancer Institute (CA-24487, J.C.) and the National Institute of General Medical Sciences (GM-38627, S.L.S.) for their support. We also gratefully acknowledge support of the area detector facility by NSF grant DIR-8820919.

References

Albers, M. W., Walsh, C. T. & Schreiber, S. L. (1990). Substrate specificity for the human rotamase FKBP: a view of FK506 and rapamycin as leucine-(twisted amide)-proline mimics. *J. Org. Chem.* **55**, 4984–4986.

Bierer, B. E., Matila, P. S., Standaert, R. F., Herzenberg, L. A., Burakoff, S. J., Crabtree, G. & Schreiber, S. L. (1990*a*). Two distinct signal transmission pathways in T lymphocytes are inhibited by complexes formed between an immunophilin and either FK506 or rapamycin. *Proc. Nat. Acad. Sci., U.S.A.* **87**, 9231–9235.

Bierer, B. E., Somers, P. K., Wandless, T. J., Burakoff, S. J. & Schreiber, S. L. (1990*b*). Probing immunosuppressant action with a nonnatural immunophilin ligand. *Science*, **250**, 556–559.

Brünger, A. T., Kuriyan, J. & Karplus, M. (1987). Crystallographic R factor refinement by molecular dynamics. *Science*, **235**, 458–460.

Brünger, A. T., Krukowski, A. & Erickson, J. (1990). Slow-cooling protocols for crystallographic refinement by simulated annealing. *Acta Crystallogr. sect. A*, **46**, 585–593.

Donald, D. K., Cooper, M. E., Furber, M., Wells, E., Hutchinson, R. & Black, F. M. (1991). C-10 N-acyl modified FK-506: a possible hybrid analog of the

transition state of peptidyl-prolyl cis-trans isomerization. *Tetra. Letters*, **32**, 1375–1378.

Fischer, C., Wittmann-Liebold, B., Lang, K., Kiefhaber, T. & Schmid, F. X. (1989). Cyclophilin and peptidyl-prolyl cis-trans isomerase are probably identical proteins. *Nature (London)*, **337**, 476–478.

Fitzgerald, P. M. D. (1988). MERLOT, an integrated package of computer programs for the determination of crystal structures by molecular replacement. *J. Appl. Crystallogr.* **21**, 273–278.

Fretz, H., Albers, M. W., Galat, A., Standaert, R. F., Lane, W. S., Burakoff, S. J., Bierer, B. E. & Schreiber, S. L. (1991). Rapamycin and FK506 binding proteins (immunophilins). *J. Amer. Chem. Soc.* **113**, 1409–1411.

Galat, A., Lane, W. S., Standaert, R. F. & Schreiber, S. L. (1992). A rapamycin-selective, 25-kDa immunophilin. *Biochemistry*, **31**, 2427–2434.

Harding, M. W., Galat, A., Uehling, D. E. & Schreiber, S. L. (1989). A receptor for the immunosuppressant FK506 is a cis-trans peptidyl-prolyl isomerase. *Nature (London)*, **341**, 758–760.

Harrison, R. K. & Stein, R. L. (1990). Mechanistic studies of peptidyl prolyl cis-trans isomerase: evidence for catalysis by distortion. *Biochemistry*, **29**, 1684–1689.

Horovitz, A., Serrano, L., Avron, B., Bycroft, M. & Fersht, A. R. (1990). Strength and cooperativity of contributions of surface salt bridges to protein stability. *J. Mol. Biol.* **216**, 1031–1044.

Howard, A. D., Nielson, C. & Xuong, Ng. H. (1985). Software for a diffractometer with multiwire area detector. In *Methods in Enzymology* (Wyckoff, H. W., Hirs, C. H. W. & Timasheff, S. N., eds), vol. 114, pp. 452–472, Academic Press, Orlando.

Jin, Y. J., Albers, M. W., Lane, W. S., Bierer, B. E., Schreiber, S. L. & Burakoff, S. J. (1991). Molecular cloning of a membrane-associated human FK506- and rapamycin-binding protein, FKPB-13. *Proc. Nat. Acad. Sci., U.S.A.* **88**, 6677–6681.

Kabsch, W. & Sander, C. (1983). Dictionary of protein secondary structure: pattern recognition of hydrogen-bonded and geometrical features. *Biopolymers*, **22**, 2577–2637.

Kallen, J., Spitzfaden, D., Zurindi, M. G. M., Wider, G., Widmer, H., Wüthrich, K. & Walkinshaw, M. D. (1991). Structure of human cyclophilin and its binding site for cyclosporin A determined by X-ray crystallography and NMR spectroscopy. *Nature (London)*, **353**, 276–279.

Karplus, P. A., Daniels, M. J. & Herriott, J. R. (1991). Atomic structure of ferredoxin-NADP+reductase: prototype for a structurally novel flavoenzyme family. *Science*, **251**, 60–66.

Ke, H., Zydowsky, L. D., Liu, J. & Walsh, C. T. (1991). Crystal structure of recombinant human T-cell cyclophilin at 2·5 Å resolution. *Proc. Nat. Acad. Sci., U.S.A.* **88**, 9483–9487.

Kofron, J. L., Kuzmic, P., Kishore, V., Colon-Bonilla, E. & Rich, D. H. (1991). Determination of kinetic constants for peptidyl prolyl cis-trans isomerases by an improved spectrophotometric assay. *Biochemistry*, **30**, 6127–6134.

Kiltin, Y., Faucette, L., Bergsma, D. J., Levy, M. A., Cafferkey, R., Koser, P. L., Johnson, R. K. & Livi, G. P. (1991). Rapamycin sensitivity in *Saccharomyces cerevisiae* is mediated by a peptidyl-prolyl cis-trans isomerase related to human FK506-binding protein. *Mol. Cell. Biol.* **11**, 1718–1723.

Liu, J., Farmer, J. D., Jr, Lane, W. S., Friedman, J., Weissman, I. & Schreiber, S. L. (1991). Calcineurin is a common target of cyclophilin-cyclosporin A and FKBP-FK506 complexes. *Cell*, **66**, 807–815.

Luzzati, V. (1952). Statistical treatment of errors in the determination of crystalline structures. *Acta Crystallogr.* **5**, 802–810.

McPherson, A., Jr (1976). The growth and preliminary investigation of protein and nucleic acid crystals for X-ray diffraction analysis. *Methods Biochem. Anal.* **23**, 249–345.

Metcalf, S. M. & Richards, F. M. (1990). Cyclosporine, FK506, and rapamycin. Some effects on early activation events in serum-free, mitogen-stimulated mouse spleen cells. *Transplantations*, **49**, 798.

Michnick, S. W., Rosen, M. K., Wandless, T. J., Karplus, M. & Schreiber, S. L. (1991). Solution structure of FKBP, a rotamase enzyme and receptor for FK506 and rapamycin. *Science*, **251**, 836–839.

Moore, J. M., Pettie, D. A., Fitzgibbon, M. J. & Thomson, J. A. (1991). Solution structure of the major binding protein for the immunosuppressant FK506. *Nature (London)*, **351**, 248–250.

Polygen Corporation (1990). *Quanta*. Version 3.0, Polygen Corporation, Waltham, MA.

Ptitsyn, D. B. & Finkelstein, A. V. (1980). Directed mechanism of the self-organization of proteins: generalized model. *Quart. Rev. Biophys.* **13**, 339–386.

Richardson, J. S. (1977). β-Sheet topology and the relatedness of proteins. *Nature (London)*, **268**, 495–500.

Rosen, M. K., Standaert, R. F., Galat, A., Nakatuska, M. & Schreiber, S. L. (1990). Inhibition of FKBP rotamase activity by immunosuppressant FK506: twisted amide surrogate. *Science*, **248**, 863–866.

Rossmann, M. G. (1975). LEASTSQ.

Sack, J. S. (1988). CHAIN—a crytallographic modeling program. *J. Mol. Graphics*, **6**, 224–225.

Scheiner, S. & Kern, C. W. (1977). Theoretical studies of environmental effects on protein conformation. *J. Amer. Chem. Soc.* **99**, 7042–7050.

Schreiber, S. L. (1991). Chemistry and biology of the immunophilins and their immunosuppressive ligands. *Science*, **251**, 283–287.

Siekierka, J. J., Hung, H. Y., Poe, M., Lin, C. S. & Sigal, N. S. (1989). A cytosolic binding protein for the immunosuppressant FK506 has peptidyl-prolyl isomerase activity but is distinct from cyclophilin. *Nature (London)*, **341**, 755–757.

Siemens Analytical X-ray Instruments, Inc. (1990). SHELXTL-PLUS, Version 4.0, Siemens Analytical X-ray Instruments, Inc., Madison, WI.

Standaert, R. F., Galat, A., Verdine, G. L. & Schreiber, S. L. (1990). Molecular cloning and overexpression of the human FK506-binding protein FKBP. *Nature (London)*, **346**, 671–674.

Swindells, D. C. N., White, P. S. & Findlay, J. A. (1978). The X-ray crystal structure of rapamycin, $C_{51}H_{79}NO_{13}$. *Can. J. Chem.* **56**, 2491–2492.

Takahashi, N., Hayano, T. & Suzuki, M. (1989). Prolylisomerase for determination of cyclosporin A or its derivatives. *Nature (London)*, **337**, 473–475.

Tanaka, H., Kuroda, A., Marusawa, H., Hatanaka, H., Kino, T., Goto, T. & Hashimoto, M. (1987). Structure of FK506, a novel immunosuppressant isolated from *Streptomyces*. *J. Amer. Chem. Soc.* **109**, 5031–5033.

Taylor, R. & Kennard, O. (1982). Crystallographic evidence for the existence of CH···O, CH···N, and CH···Cl hydrogen bonds. *J. Amer. Chem. Soc.* **104**, 5063–5070.

Thaller, C., Weaver, L. H., Eichele, G., Wilson, E., Karlsson, R. & Jansonius, J. N. (1981). Repeated seeding technique for growing large single crystals of proteins. *J. Mol. Biol.* **147**, 465–469.

Thomas, K. A., Smith, G. M., Thomas, T. B. & Feldmann, R. J. (1982). Electronic distributions within protein phenylalanine aromatic rings are reflected by the three-dimensional oxygen atom environments. *Proc. Nat. Acad. Sci., U.S.A.* **79**, 4843–4847.

Thomson, A. W. (1989). FK506—How much potential? *Immunol. Today*, **10**, 6.

Van Duyne, G. D., Standaert, R. F., Karplus, P. A., Schreiber, S. L. & Clardy, J. (1991*a*). Atomic structure of FKBP-FK506, an immunophilin-immunosuppressant complex. *Science*, **252**, 839–842.

Van Duyne, G. D., Standaert, R. F., Schreiber, S. L. & Clardy, J. (1991*b*). Atomic structure of the rapamycin human immunophilin FKBP-12 complex. *J. Amer. Chem. Soc.* **113**, 7433–7434.

Venkatachalam, C. M. (1968). Stereochemical criteria for polypeptides and proteins. V. Conformation of a system of three-linked peptide units. *Biopolymers*, **6**, 1425–1436.

Wiberg, K. B. & Laidig, K. E. (1987). Barriers to rotation adjacent to double bonds. 3. The carbon-oxygen barrier in formic acid, methyl formate, acetic acid, and methyl acetate. The origin of ester and amide resonance. *J. Amer. Chem. Soc.* **109**, 5935–5943.

Wiberg, K. B., Waldron, R. F., Schulte, G. & Saunders, M. (1991). Lactones. 1. X-ray crystallographic studies of nonanolactone and tridecanolactone: nature of CH···O nonbonded interactions. *J. Amer. Chem. Soc.* **113**, 971–977.

Wlodawer, A., Diesenhofer, J. & Huber, R. (1987). Comparison of two highly refined structures of bovine pancreatic trypsin inhibitor. *J. Mol. Biol.* **193**, 145–156.

Yang, W., Hendrickson, W. A., Kalman, E. T. & Crouch, R. J. (1990). Expression, purification, and crystallization of natural and selenomethionyl recombinant ribonuclease H from *Escherichia coli*. *J. Biol. Chem.* **265**, 13553–13559.

Edited by W. Hendrickson

THE JOURNAL OF BIOLOGICAL CHEMISTRY
Vol. 273, No. 26, Issue of June 26, pp. 16621–16629, 1998
Printed in U.S.A.

Regulation of the p70 S6 Kinase by Phosphorylation in Vivo

ANALYSIS USING SITE-SPECIFIC ANTI-PHOSPHOPEPTIDE ANTIBODIES*

(Received for publication, February 20, 1998, and in revised form, April 6, 1998)

Qing-Ping Weng‡, Mark Kozlowski‡, Christopher Belham‡, Aihua Zhang§, Michael J. Comb§, and Joseph Avruch‡¶

From the ‡Diabetes Unit and Medical Services and the Department of Molecular Biology, Massachusetts General Hospital and the Department of Medicine, Harvard Medical School, Boston, Massachusetts 02114 and §New England Biolabs, Beverley, Massachusetts 01915

The p70 S6 kinase is activated by diverse stimuli through a multisite phosphorylation directed at three separate domains as follows: a cluster of (Ser/Thr) Pro sites in an autoinhibitory segment in the noncatalytic carboxyl-terminal tail; Thr-252 in the activation loop of the catalytic domain; and Ser-394 and Thr-412 in a segment immediately carboxyl-terminal to the catalytic domain. Phosphorylation of Thr-252 in vitro by the enzyme phosphatidylinositol 3-phosphate-dependent kinase-1 or mutation of Thr-412 3 Glu has each been shown previously to engender some activation of the p70 S6 kinase, whereas both modifications together produce 20–30-fold more activity than either alone. We employed phospho-specific anti-peptide antibodies to examine the relative phosphorylation at several of these sites in wild type and various p70 mutants, in serum-deprived cells, and in response to activators and inhibitors of p70 S6 kinase activity.

Substantial phosphorylation of p70 Thr-252 and Ser-434 was present in serum-deprived cells, whereas Thr-412 and Thr-444/Ser-447 were essentially devoid of phospho-specific immunoreactivity. Activation of p70 by insulin was accompanied by a coordinate increase in phosphorylation at all sites examined, together with a slowing in mobility on SDS-PAGE of a portion of p70 polypeptides. Upon addition of rapamycin or wortmannin to insulin-treated cells, the decrease in activity of p70 was closely correlated with the disappearance of anti-Thr-412(P) immunoreactivity and the most slowly migrating p70 polypeptides, whereas considerable phosphorylation at Ser-434 and Thr-252 persisted after the disappearance of 40 S kinase activity. The central role of Thr-412 phosphorylation in the regulation of kinase activity was further demonstrated by the close correlation of the effects of various deletions and point mutations on p70 activity and Thr-412 phosphorylation.

In conclusion, although p70 activity depends on a disinhibition from the carboxyl-terminal tail and the simultaneous phosphorylation at both Thr-252 and Thr-412, p70 activity in vivo is most closely related to the state of phosphorylation at Thr-412.

The p70 S6 kinase, an enzyme critical for cell cycle progression through G_1, was among the first insulin/mitogen-activated protein (Ser/Thr) kinases to be identified, purified, and molecularly cloned. The enzyme was shown early on to be regulated by insulin/mitogen-stimulated (Ser/Thr) phosphorylation, and along with the kinases now known as Rsk provided the first evidence that insulin/mitogen signal transduction involved the recruitment of multiple, independently regulated cascades of protein (Ser/Thr) kinases (reviewed in Ref. 1). Nevertheless, whereas the in vitro activation of Rsk kinases by mitogen-activated protein kinase-catalyzed phosphorylation was accomplished early on (2), in vitro activation of p70 S6 kinase has proved much more difficult to reconstruct. During activation in vivo, p70 is phosphorylated at 10 or more sites by an array of independently regulated protein kinases. Enumerating the sites of phosphorylation, determining their individual functional roles in the process of p70 activation as well as the potential site-site interactions, has provided a formidable challenge. Work to date has identified four sets of phosphorylation sites on p70 that undergo insulin or mitogen-stimulated phosphorylation in situ, and whose mutation affects substantially p70 kinase activity. The first to be characterized were a cluster of 4–5 residues (Ser-434, Ser-441, Ser-447, Ser-452, and Thr-444) situated within an autoinhibitory pseudosubstrate segment in the p70 noncatalytic tail (3–6); conversion of 434, 441, 444, and 447 to Ala suppresses mitogen-stimulated p70 activation, whereas conversion to Asp and Glu increases basal p70 activity (7). The phosphorylation of Thr-252 in the p70 activation loop within the catalytic domain is stimulated by serum and PI-3 kinase[1] overexpression in vivo and is inhibited by wortmannin, and only a Ser or Thr at this site enables p70 activity (8). Thr-412 is another site of mitogen-stimulated phosphorylation, situated in a conserved 65-amino acid segment located immediately carboxyl-terminal to the catalytic domain; conversion of Thr-412 to Ala strongly suppresses p70 activity, whereas conversion to Glu increases basal activity and restores mitogen responsiveness (7, 9). Most recently Ser-394, which like Thr-412 is also located in the catalytic domain carboxyl-terminal extension, has also been shown to influence p70 activity (10). As to the kinases that act on these sites, the sites clustered in the carboxyl-terminal tail (Ser-434, Ser-441, Ser-447, Ser-452, and Thr-444) are each followed immediately by a proline residue and can be phosphorylated in vitro by an array of proline-directed kinases, including Erk1 and Erk2, the stress-activated protein kinases, and Cdc2 (the latter acting particularly at Ser-434) (5). Ser-394 is also followed by a pro-

* This work was supported by National Institutes of Health Grant DK17776. The costs of publication of this article were defrayed in part by the payment of page charges. This article must therefore be hereby marked "advertisement" in accordance with 18 U.S.C. Section 1734 solely to indicate this fact.

¶ To whom correspondence should be addressed: Diabetes Research Laboratory, Dept. of Molecular Biology, Massachusetts General Hospital, 50 Blossom St., Boston, MA 02114. Tel.: 617-726-6909; Fax: 617-726-5649; E-mail: avruch@helix.mgh.harvard.edu.

[1] The abbreviations used are: PI-3 kinase, phosphatidylinositol 3-kinase; CHO-IR, Chinese hamster ovary-insulin receptor; HA, hemagglutinin; PDK, phosphatidylinositol 3-phosphate-dependent kinase; PAGE, polyacrylamide gel electrophoresis; PtdIns(3,4,5)P_3, phosphatidylinositol (3,4,5)-trisphosphate.

line and may also be a substrate for these kinases. Nevertheless, phosphorylation of PP2A-treated p70 in vitro with one or several proline-directed kinases does not restore any p70 S6 kinase activity (5).

Recently, the kinase PDK1 was shown to phosphorylate p70 in vitro selectively at Thr-252, with a resultant increase in p70 S6 kinase activity (11, 12). This finding together with the earlier demonstration of PI-3 kinase-stimulated, wortmannin-sensitive Thr-252 phosphorylation in vivo (8) establishes Thr-252 as a critical site of regulatory phosphorylation. Nevertheless, both the ability of p70 to be phosphorylated by PDK1 and the relative and absolute extent of p70 activation engendered by PDK1-catalyzed phosphorylation are greatly altered by a variety of p70 mutations (11). Thus conversion of the five clustered (Ser/Thr-Pro) phosphorylation sites in the p70 carboxyl-terminal tail to Ala strongly suppresses PDK1-catalyzed Thr-252 phosphorylation, whereas deletion of the entire carboxyl-terminal tail (to give p70• CT104) increases both the rate and extent of Thr-252 phosphorylation by PDK1 and also the degree of S6 kinase activation achieved at any level of Thr-252 phosphorylation. Deletion of p70 amino-terminal noncatalytic residues 2–46, a modification previously shown to greatly inhibit p70 activity, essentially abolishes the ability of p70 to be phosphorylated by PDK1 in vitro, whereas the additional deletion of the carboxyl-terminal tail (to give • 2–46/• CT104), which restores p70 activity and mitogen responsiveness in vivo, also restores the ability of PDK1 to catalyze p70 Thr-252 phosphorylation in vitro. These results indicate that the p70 carboxyl-terminal tail exerts a strong influence on both the ability of PDK1 to catalyze the phosphorylation of Thr-252, as well as the extent of activation of S6 kinase activity resulting therefrom (11).

As regards the other sites of p70 phosphorylation, Thr-412 appears to play an especially important role, in that it influences both the ability of PDK1 to phosphorylate Thr-252 in vitro and the absolute extent of p70 activity that results from Thr-252 phosphorylation (11). Thus, conversion of Thr-412 in p70• CT104 to either Ala or Glu facilitates PDK1-catalyzed Thr-252 phosphorylation in vitro. Moreover, the functional interaction of Thr-252(P) and Thr-412 is the major, perhaps predominant, factor in determining p70 activity. Thus, whereas protein phosphatase 2A ($PP2A_1$)-treated p70• CT104 is essentially inactive, the selective phosphorylation of p70• CT104 at Thr-252 by PDK1 results in a 15-fold increase in 40 S kinase activity to a level comparable to that exhibited by $PP2A_1$-treated p70• CT104 (Thr-412 3 Glu). This indicates that modification of either Thr-252 or Thr-412 singly is sufficient to confer some S6 kinase activity. This activity, however, represents no more than 3–5% of maximal S6 kinase activity, inasmuch as PDK1 phosphorylation of $PP2A_1$-treated p70• CT104(T412E) increases its S6 kinase activity by a further 20–30-fold, to a level 240-fold greater than that exhibited by $PP2A_1$-treated (i.e. fully dephosphorylated) p70• CT104, demonstrating clearly the strong positive cooperativity between Thr-252 and Thr-412 in p70 activation (11). Thus, the phosphorylation state of the p70 carboxyl-terminal tail and Thr-412 both strongly influence the rate and extent of p70 Thr-252 phosphorylation catalyzed by PDK1 in vitro, as well as the absolute level of 40 S kinase activity engendered by a given extent of Thr-252 phosphorylation.

These data, derived for PDK1-catalyzed p70 phosphorylation in vitro, strongly suggest that any significant activation of S6 kinase in vivo requires the concurrent phosphorylation of both Thr-412 and Thr-252; the relevance of these in vitro data to p70 regulation in vivo as well as the determinants of Thr-252 and Thr-412 phosphorylation in vivo remain to be fully defined. To explore these questions we have employed anti-phosphopeptide antibodies developed toward several of the functionally important p70 phosphorylation sites as follows: Thr-412(P), Thr-252(P), Ser-434(P), and the cluster Ser-444(P)/Thr-447(P). These antibodies were used to examine the effects of insulin, recombinant PI-3 kinase, wortmannin, and rapamycin as well as the effects of p70 truncations and point mutations on site-specific p70 phosphorylation in vivo. We have attempted to correlate the changes in p70 S6 kinase activity with the site-specific phosphorylation, to verify whether the potent site-site interactions detected with in vitro phosphorylation obtain in vivo, and to identify which phosphorylation events determine S6 kinase activity during activation and deactivation in vivo.

MATERIALS AND METHODS

Dulbecco's modified Eagle's medium, fetal bovine serum, and chemicals were obtained from Sigma. Ham's F-12 medium, LipofectAMINE, and protein G-agarose were purchased from Life Technologies, Inc. Restriction enzymes were products of New England Biolabs. [•-^{32}P]ATP, anti-rabbit Ig-linked horseradish peroxidase, and ECL were from Amersham Pharmacia Biotech.

Construction of p70 S6 Kinase Mutant Expression Vectors—A pMT2-based cDNA encoding an amino-terminal HA-tagged p70 •I and mutant proteins p70• CT104, p70• 2–46, p70• 2–46/• CT104, K123M, and T252A was described previously (13). Site-specific mutants p70T412A, T412E, • 2–46/T412A, • 2–46/T412E, T434A, T444A/S447A, S394A, and S394D were generated using a polymerase chain reaction-based method. The mutations were verified by DNA sequence and restriction analysis for newly introduced diagnostic restriction sites (11).

Transient Expression and Immunopurification of the p70 S6 Kinase—HEK293 cells and CHO-IR cells were maintained in Dulbecco's modified Eagle's medium and Ham's F12 medium supplemented with 10% fetal bovine serum, respectively. HEK293 cells were transfected at 60% confluence in 100-mm dishes by the calcium phosphate method using 5 • g of plasmid DNA encoding wild type or variant p70. CHO-IR cells in 60-mm dishes were transfected with 1–2 • g of plasmid DNA using LipofectAMINE according to the manufacturer's protocol (Life Technologies, Inc.). Twenty four hours post-transfection, cells were placed in serum-free medium for 16 h and then treated with insulin or 20% serum for the times indicated; in some experiments, rapamycin (50 nM) or wortmannin (100 nM) was added 10 min after insulin. Incubations were terminated by two rapid rinses with ice-cold phosphate-buffered saline; the cells were then extracted with lysis buffer (13) and centrifuged at 12,000 • g for 10 min. Aliquots of supernatants were matched for protein content, and HA p70 polypeptides were immunoprecipitated by addition of the monoclonal anti-HA epitope antibody 12CA5 and protein-G agarose at 4 °C for 3 h. The beads were washed three times with lysis buffer, once with 1 M NaCl in lysis buffer, and once with kinase reaction buffer. Endogenous p70 was immunoprecipitated using a rabbit polyclonal antiserum generated against a recombinant fragment encoding p70 amino acids 422–525 (14).

S6 Kinase Assay—The immunocomplexes of the p70 S6 kinase were used to assay for p70 kinase activity using 40 S ribosomal subunit as described previously (13). The reaction mixtures were separated by sodium dodecyl sulfate-polyacrylamide gel electrophoresis (SDS-PAGE) and transferred a polyvinylidene difluoride membrane (Millipore Corp.), which was subjected to autoradiography for the detection of ^{32}P-S6, and immunoblot analysis.

Anti-phosphopeptide Antibody Production—Phospho-specific antibodies directed against the various sites of p70 S6 kinase were produced by immunizing New Zealand White rabbits with the following synthetic phosphopeptides coupled to keyhole limpet hemocyanin: Thr-252(P) (IHDGTVTHT*FCGTI), Thr-412(P) (NQVFLGFT*YVAPKKC), Ser-434(P) (EPKIRS*PRRFIGC), and Thr-444(P)/Ser-447(P) (SPRT*PVS*PVKFSC). Enzyme-linked immunosorbent assay, using the phosphopeptide and corresponding nonphosphopeptide, was employed to identify the rabbits responding best. IgG was purified using protein A-Sepharose. Antibodies reactive with the nonphosphopeptide were removed by adsorption to a nonphosphopeptide (same sequence as above) affinity column. Antibodies that flowed through this column were next passed over a column of immobilized phosphopeptide; after washing, antibodies were eluted at low pH and dialyzed; these are subsequently referred to as "type 1" antibodies. The resulting antibodies were characterized by enzyme-linked immunosorbent assay against phospho- and nonphosphopeptides to determine the extent of phospho-specificity and subsequently by Western blotting to examine specificity

against whole cell extracts. "Type 2" antibodies (seen only with the Thr-252(P) peptide immunogen) were those that bound to the affinity column that contained the nonphosphorylated peptide but showed little or no reactivity on immunoblot with a p70 Thr-252 3 Ala mutant polypeptide (see "Results" and Fig. 1C).

Immunoblot Analysis of Phospho p70 Polypeptides—The electroblotted p70 polypeptides were analyzed using a standard Western blot protocol. Briefly, the membrane was first blocked with 5% low-fat milk in TBST-T (20 mM Tris-HCl, pH 7.6, 137 mM NaCl, 0.2% Tween 20) at room temperature for 1 h, rinsed once with TBS-T, and probed with anti-phosphopeptide antibody at (0.02–0.05 • g/ml) in TBS-T for 1 h. Following three 20-min washes, the membranes were incubated with a horseradish peroxidase-labeled anti-IgG for 1 h at room temperature, followed by three 20-min washes with TBS-T. The membrane was wetted in ECL solution for 3 min, exposed to x-ray film, and developed. For sequential immunoblot analysis, the membranes were stripped in 2% SDS, 62.5 mM Tris-HCl, pH 6.8, 100 mM 2-mercaptoethanol at 50 °C for 30 min, washed extensively with TBS-T, and reused.

RESULTS

The anti-p70 phosphopeptide antibodies were generated by immunization of female New Zealand White rabbits with synthetic phosphopeptide covalently coupled to keyhole limpet hemocyanin. The presence of phosphopeptide-specific immunoreactivity was detected by enzyme-linked immunosorbent assay using both the phosphorylated and nonphosphorylated peptides. After purification of IgG with protein A-agarose, the phosphopeptide-specific antibodies were purified by first passing the IgG over immobilized, nonphosphorylated peptide to remove antibodies reactive with nonphosphorylated epitopes; the nonadsorbed fraction was then passed over a column of immobilized phosphopeptide. After extensive washing, the retained immunoglobulins were eluted at low pH, rapidly neutralized, dialyzed, and concentrated. In this manner phosphopeptide-specific antibodies toward Thr-412(P), Thr-434(P), and the doubly phosphorylated peptide containing Thr-444(P)/Ser-447(P) were isolated.

The ability of each of these anti-p70 phosphopeptide antibodies to immunoblot recombinant p70 polypeptides was compared with an antibody prepared to a synthetic peptide corresponding to p70 amino acids 337–352, which contains no Ser or Thr residues (14). As is evident in Fig. 1A, this anti-p70 peptide antibody exhibits comparable reactivity with each of the recombinant wild type and mutant p70 polypeptides that is unaffected by insulin or serum treatment prior to extraction. The anti-p70 phosphopeptide antibodies react with all p70 variants except those wherein the Ser and/or Thr residue that was phosphorylated in the synthetic peptide antigen has been mutated to a nonphosphorylatable residue (Ala, Glu, or Asp). These features indicate that the anti-(Thr-412(P)), anti-(Thr-444(P)/Ser-447(P)), and anti-(Ser-434(P)) antibodies each are indeed specific for the peptide segment containing only a phosphorylated Ser and/or Thr. In addition, and to a varying extent, the immunoreactivity of each of these anti-p70 phosphopeptide antibodies is increased by insulin treatment prior to extraction.

As regards the anti-p70 Thr-252(P) antibodies, some sera (type 1) yielded anti-phosphopeptide antibodies with properties identical to those described above, i.e. nonadsorption to unphosphorylated peptide, adsorption to the phosphopeptide, and reactivity with wild type p70 but not with a p70 (Thr-252 3 Ala) mutant polypeptide (Fig. 1B). These antibodies were, however, recovered in low yield, insufficient to complete the studies required. A second type of anti-(Thr-252(P)) antibody was found to adsorb to columns containing the immobilized nonphosphorylated peptide. These antibodies, when eluted from the peptide column, also showed highly selective reactivity with wild type p70 polypeptide over the p70 (Thr-252 3 Ala), as well as a stimulus-dependent increase in immunoreactivity (Fig. 1C). It is not clear whether these type 2 antibodies are directly reactive with Thr-252(P) itself; conceivably, these antibodies may react with a conformationally dependent epitope on the activation loop that is generated as a consequence of Thr-252 phosphorylation but does not include the Thr-252(P) residue itself. This epitope must be highly dependent on Thr-252 phosphorylation inasmuch as the p70 (Thr-256 3 Ala) mutant, which like the p70 (Thr-252 3 Ala) mutant, is completely inactive, nevertheless exhibits an unimpaired insulin-stimulated increase in immunoreactivity with the type 2 anti-(Thr-252(P)) antibodies (Fig. 5B), a finding similar to that seen previously with ^{32}P labeling in vivo (8). In practice, therefore, both types of anti-p70 (Thr-252(P)) antibodies provide a reliable monitor of the state of Thr-252 phosphorylation, even though the type 2 anti-p70 (Thr-252(P)) antibodies also have some reactivity with an epitope(s) present in the nonphosphorylated peptide segment.

Having defined the specificity of these antisera, we next examined the effects of serum (in 293 cells), insulin (in CHO-IR cells), or cotransfection with various candidate upstream activators on the 40 S kinase activity and site-specific phosphorylation of full-length, p70• 1 polypeptides expressed transiently in 293 cells or CHO-IR cells. Insulin elicited a rapid 3–4-fold increase in 40 S kinase activity in CHO-IR cells, which attained 60% of maximal by the first time point examined, 2.5 min after insulin addition. All sites exhibited an increase in phosphorylation, with the largest relative increases observed with Thr-412 and Thr-444/Ser-447, primarily because these sites contain little or no detectable phosphate in serum-deprived cells (Fig. 2A). Thr-252 exhibits clear-cut basal phosphorylation, which nevertheless rapidly increases after insulin addition in parallel with the increased S6 kinase activity. Thus, even after the addition of submaximal concentrations of insulin, the increase in overall phosphorylation at all sites is comparably rapid, such that it cannot be reliably inferred from such data as to whether p70 phosphorylation occurs in an ordered sequence.

Given the relatively concerted phosphorylation in vivo of the wild type p70 after insulin addition, we attempted to evaluate the pattern of dephosphorylation that accompanies inhibition of p70 in vivo after addition of rapamycin or wortmannin, each added 10 min after the addition of insulin (Fig. 2B). Rapamycin led to the rapid inactivation of p70, with dephosphorylation evident at all sites, accompanied by a striking downshift, i.e. increase in p70 mobility on SDS-PAGE. The decrease in 40 S kinase activity, the disappearance most slowly migrating immunoreactive p70 polypeptide band (best seen in the anti-p70 (Thr-444(P)/Ser-447(P)) blot), and the disappearance of overall anti-(Thr-412(P)) immunoreactivity were each entirely congruent. Thr-252(P) immunoreactivity also diminished, but slightly more slowly, and did not disappear; this slower response was paralleled by the pattern seen with anti-(Ser-434(P)) immunoreactivity. The response to wortmannin, although somewhat slower, was also characterized by the concomitant disappearance of 40 S kinase activity, the most slowly migrating immunoreactive p70 polypeptide band, and total anti-p70 (Thr-412(P)) immunoreactivity, with somewhat slower and less pronounced dephosphorylation of Thr-252 and Ser-434.

These properties of recombinant p70 expressed in CHO-IR cells were compared with the behavior of the p70 polypeptide endogenous to these cells. Each of the anti-phosphopeptide antisera was sufficiently sensitive to dependably monitor the phosphorylation of the endogenous p70 except for the various anti-p70 (Thr-252(P)) antisera, whose sensitivity was at the limit of detection; visualization of p70 Thr-252(P) was therefore not achieved in every experiment. Given this limitation, insulin, after a brief lag, promoted the coordinate phosphorylation

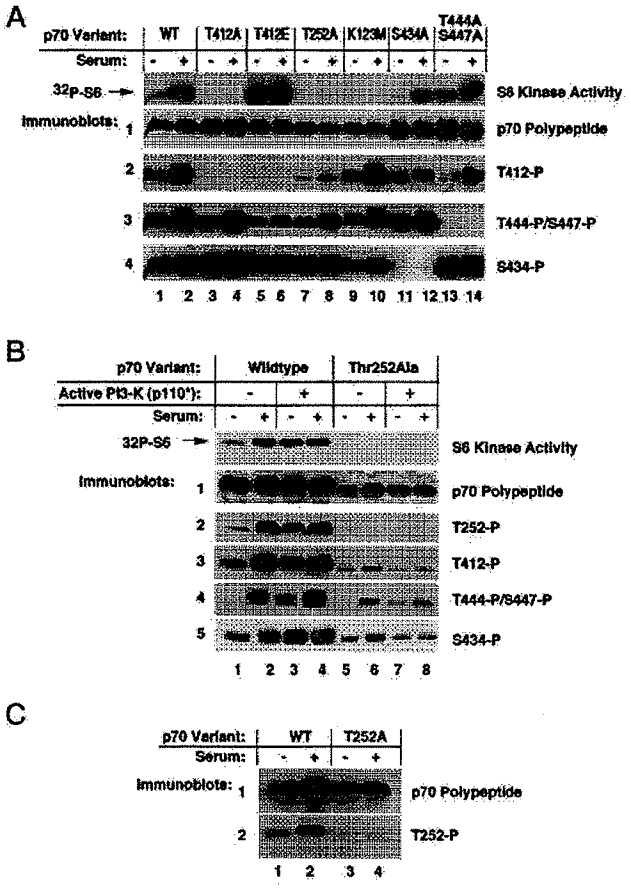

FIG. 1. Characterization of anti-p70 phosphopeptide antibodies. A, the specificity of various anti-p70 phosphopeptide antibodies. HEK-293 cells were transfected with plasmids encoding HA-tagged p70•1 wild type (WT, lanes 1 and 2) or HA p70•1 containing the point mutations Thr-412 → Ala (T412A, lanes 3 and 4); Thr-412 → Glu (T412E, lanes 5 and 6); Thr-252 → Ala (T252A, lanes 7 and 8); Lys-123 → Met (K123M, lanes 9 and 10); Ser-434 → Ala (S434A, lanes 11 and 12); and a double mutant, Thr-444 → Ala/Ser-447 → Ala (T444A,S447A, lanes 13 and 14). After 36 h, the cells were deprived of serum and 12 h later treated with medium (lanes 1, 3, 5, 7, 9, 11, and 13) or 10% serum (lanes 2, 4, 6, 8, 10, 12, and 14) for 20 min prior to harvest. Cell extracts matched for protein were immunoprecipitated with a monoclonal anti-HA antibody, 12CA5. Washed immunoprecipitates were assayed for S6 kinase activity (^{32}P-S6) and subjected to SDS-PAGE followed by electrophoretic transfer to a polyvinylidene difluoride membrane. Immunoblots using the following antisera were carried out. 1, anti-p70 peptide (amino acids 332–353); 2, anti-T412P, anti-p70 phosphopeptide (amino acids 405–416 Thr-412(P); 3, anti-T444P/ S447P, anti-p70 phosphopeptide (amino acid 441–452, Thr-444(P)/Ser-447(P); 4, anti-S434P, anti-p70 phosphopeptide (amino acids 429–440; anti-S434P). The actual ^{32}P cpm incorporated into S6 in the kinase assay shown were: lane 1, 1022; lane 2, 7872; lane 3, 164; lane 4, 88; lane 5, 9393; lane 6, 14324; lane 7, 259; lane 8, 219; lane 9, 300; lane 10, 89; lane 11, 316; lane 12, 2930; lane 13, 2901; lane 14, 7168. B, the specificity of type 1 anti-p70 phosphopeptide (amino acids 244–257, Thr-252(P)) antibodies. HEK293 cells were transfected with either HA p70•1 wild type (lanes 1–4) or a mutant p70 (Thr-252 → Ala, lanes 5–8), singly (lanes 1, 2, 5, and 6) or together with a plasmid encoding a mutant, constitutively active p110 catalytic subunit of the PI-3 kinase (lanes 3, 4, 7, and 8). After 36 h, medium (lane 1, 3, 5, and 7) or serum (to 10%, lanes 2, 4, 6, and 8) was added and the cells were harvested 20 min later. Anti-HA immunoprecipitates were assayed for S6 kinase (^{32}P-S6) and subjected to immunoblot with the antibodies used in A and, in addition, with type 1 anti-p70 phosphopeptide (Thr-252(P)) antibody. The actual ^{32}P cpm incorporated into S6 in the kinase assay shown are as follows: lane 1, 2397; lane 2, 8089; lane 3, 7332; lane 4, 8079; lane 5, 519; lane 6, 169; lane 7, 94; lane 8, 46. C, the specificity of type 2 anti-p70 phosphopeptide (amino acids 244–257 Thr-252(P)) antibodies. HEK293 cells transiently expressing HA p70 wild type (lanes 1 and 2) HA or p70 Thr-252 → Ala (lanes 3 and 4) were treated with 10% serum and extracted, and anti-HA immunoprecipitates were prepared as described in A. These were subjected to SDS-PAGE followed by immunoblot with anti-p70 peptide (amino acids 332–353) antibody (panel 1) or type 2 anti-p70 phosphopeptide (amino acids 244–257, Thr-252(P)) antibodies (panel 2).

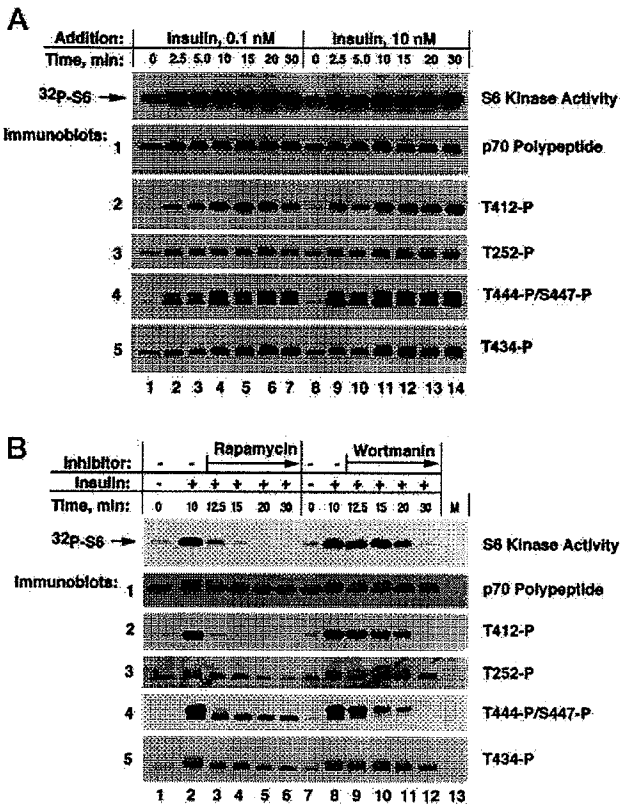

FIG. 2. The relation of S6 kinase activity and site-specific phosphorylation of recombinant p70•1 in CHO-IR cells. A, time course of insulin-stimulated activation and site-specific phosphorylation of p70 S6 kinase. CHO cells stably overexpressing human insulin receptor (CHO-IR cells) were transfected with pMT2 HA p70. Thirty six hours later, the cells were deprived of serum. After 12 h, carrier (lanes 1 and 8) or insulin was added to a final concentration of 0.1 nM (lanes 2–7) or 10 nM (lanes 2–14). The time elapsed from addition of insulin to extraction is shown. Aliquots of extracts containing equal protein were subjected to anti-HA immunoprecipitation followed by assay for S6 kinase (^{32}P-S6) and immunoblot with the antibodies indicated. ^{32}P cpm into S6, lane 1, 1250; lane 2, 3068; lane 3, 3461; lane 4, 4262; lane 5, 4163; lane 6, 4690; lane 7, 3600; lane 8, 1483; lane 9, 3590; lane 10, 3585; lane 11, 4453; lane 12, 3725; lane 13, 3527; lane 14, 3581. B, effect of rapamycin and wortmannin on the site-specific phosphorylation of insulin-activated recombinant p70 in CHO-IR cells. CHO-IR cells expressing HA p70•1 were deprived of serum and 12 h later treated with carrier (lanes 1 and 7) or insulin (10^{-7} M, lanes 2–6 and 8–12). 10 min after the addition of insulin, rapamycin (200 nM, lanes 3–6) or wortmannin (0.1 • M, lanes 9–12) was added, and cells were extracted at the times indicated over the next 20 min. The anti-HA immunoprecipitates were assayed for S6 kinase activity (^{32}P-S6) and subjected to immunoblot using antibodies indicated. Type 2 anti-Thr-252(P) antibodies were used. ^{32}P cpm into S6: lane 1, 1312; lane 2, 5080; lane 3, 1821; lane 4, 1032; lane 5, 393; lane 6, 248; lane 7, 1524; lane 8, 5474; lane 9, 4884; lane 10, 4366; lane 11, 2736; lane 12, 961.

of Thr-444/Ser-447 and Thr-412 concomitant with activation of 40 S kinase; the phosphorylation of Ser-434 increased somewhat more slowly (Fig. 3A). Deactivation of p70 by wortmannin or rapamycin was paralleled by the dephosphorylation of Thr-412(P) and Thr-444(P)/Ser-447(P), whereas phosphorylation at the other sites including Thr-252, although decreased substantially by both inhibitors, was better preserved than 40 S activity or Thr-412 phosphorylation (Fig. 3B). In addition, the disappearance of 40 S kinase and anti-Thr-412(P), Thr-444(P)/

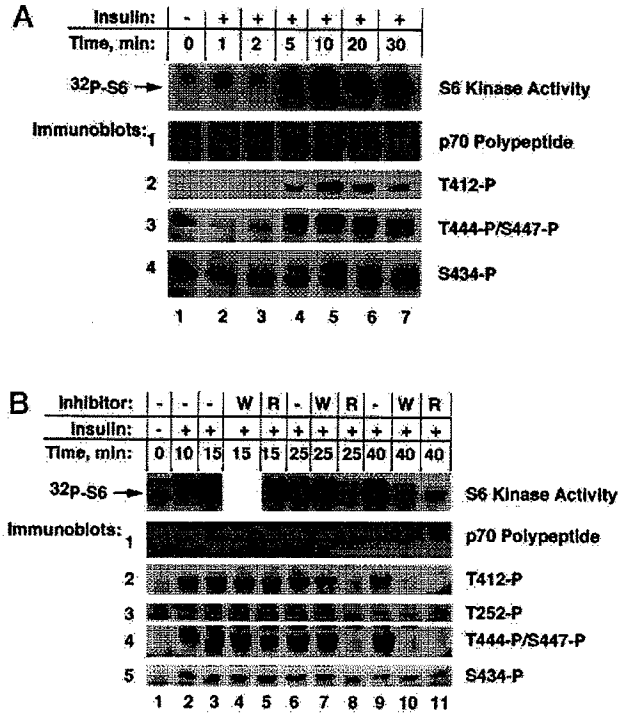

FIG. 3. The relation of site-specific phosphorylation of p70 S6 kinase endogenous to CHO-IR cells to S6 kinase activation and deactivation. A, time course of insulin activation. Serum-deprived CHO-IR cells were treated with carrier (lane 1) or insulin (10^{-7} M, lanes 2–7), and the cells were harvested thereafter at times indicated. The p70 polypeptide was immunoprecipitated with an antibody to the carboxyl-terminal tail (amino acids 422–525); the immunoprecipitates were assayed for S6 kinase activity (^{32}P-S6) and immunoblotted with the antibodies indicated. B, site-specific phosphorylation of p70 endogenous to CHO-IR cells after addition of rapamycin or wortmannin to insulin-stimulated cells. Serum-deprived CHO-IR cells were treated with insulin (10^{-7} M, lanes 2–11). Ten minutes later, rapamycin (50 nM, lanes 5, 8, and 11) or wortmannin (100 nM, lanes 4, 7, and 10) was added. Extracts were prepared at the times indicated and anti-p70 (carboxyl-terminal 422–525) immunoprecipitates were analyzed for S6 kinase activity (^{32}P-S6) and by immunoblot using the antibodies indicated; type 2 anti-Thr-252(P) antibodies were used. The S6 kinase assay sample in lane 4 was lost.

Ser-447(P) immunoreactivity is associated with a slightly faster mobility on SDS-PAGE of the residual immunoreactive bands visualized by the anti-Thr-252(P) and anti-Thr-434(P) antibodies (Fig. 3B). Thus, the regulation and phosphorylation of recombinant and endogenous p70 in CHO-IR appears quite similar. Based on this fidelity, we next examined the regulation of a variety of p70 truncation and point mutations.

Deletion of the p70 carboxyl-terminal tail (amino acids 422–525) has little effect on Thr-412 phosphorylation but substantially diminishes the phosphorylation of Thr-252; the 40 S kinase activity of p70• CT104, however, is very similar to that of the full-length enzyme. Inasmuch as previous work has shown that the activity of p70• CT104, as with full-length p70, requires Thr-252 phosphorylation (8), we infer that the efficiency of Thr-252 and/or Thr-412 phosphorylation in causing activation of 40 S kinase is enhanced by deletion of the carboxyl-terminal tail. Deletion of the p70 amino-terminal segment • 2–46 has been shown previously to greatly diminish 40 S kinase activity (13). As seen in Fig. 4A, the • 2–46 deletion is accompanied by a marked reduction in Thr-252 phosphorylation comparable to that seen with carboxyl-terminal deletion; in contrast to • CT104, the • 2–46 deletion causes a virtually complete abolition of Thr-412 phosphorylation. Further deletion of the carboxyl-terminal tail (to give • 2–46/• CT104) restores insulin-stimulated 40 S kinase nearly completely, concomitant with the restoration of insulin-stimulated Thr-412 phosphorylation; Thr-252 phosphorylation, however, remains at the low level seen with either of the single deletions. These results suggest that the low activity accompanying the • 2–46 deletion is attributable to a failure of Thr-412 (rather than Thr-252) phosphorylation. Support for this conclusion is provided by the ability of a Thr-412 3 Glu mutation to overcome almost completely the inhibitory effect of • 2–46, despite the continued presence of the carboxyl-terminal tail; conversion of • 2–46 p70 (Thr-412) to Glu restores both 40 S kinase activity and Thr-252 phosphorylation (Fig. 4B). The • 2–46/• CT104 double deletion mutant, although activated in vivo by insulin and inhibited by wortmannin, is almost completely resistant to inhibition by rapamycin (13). This correlates with the inability of rapamycin to reverse the mitogen-stimulated phosphorylation at Thr-412 in the • 2–46/• CT104 variant, whereas wortmannin, presumably via inhibition of PI-3 kinase, causes the dephosphorylation of p70 Thr-412 and inactivation of • 2–46/• CT104 (15). These findings indicate that the ability of rapamycin to inactivate wild type p70 through the dephosphorylation of p70 Thr-412 is not attributable to a rapamycin-induced inhibition of the PtdIns(3,4,5)P_3-regulated kinases that act on Thr-412.

We next examined the effects of p70 point mutations on 40 S kinase activity and site-specific phosphorylation. Mutation of Lys-123 to methionine inactivates 40 S kinase activity completely but does not alter the pattern of basal or stimulated p70 phosphorylation, indicating that none of the insulin-stimulated p70 phosphorylations reflect (cis) autophosphorylation (Figs. 1A and 5B). As described above, Thr-256, a nonphosphorylated residue in the p70 activation loop, when converted to Ala, also inactivates the 40 S kinase activity without affecting p70 phosphorylation (Fig. 5B). In contrast, conversion of Thr-252 to Ala, in addition to abolishing the 40 S kinase activity, reduces the phosphorylation at Thr-412 to a great extent without affecting phosphorylation at sites within the carboxyl-terminal tail (Fig. 1A).

Reciprocally, mutation of Thr-412 to Ala abolishes 40 S kinase activity and Thr-252 phosphorylation (Fig. 5A) with little effect on Ser-434, Thr-444, or Ser-447 phosphorylation (Fig. 1A). Thus, whereas the truncation experiments indicate that the carboxyl-terminal tail influences strongly the phosphorylation at Thr-412 and Thr-252, inactivating mutations at either of these two residues, although each inhibiting phosphorylation at the other site, do not alter phosphorylation at the carboxyl-terminal sites. Mutation of Thr-412 to Glu results in a substantial activation of 40 S kinase activity in serum-deprived cells (Fig. 1A), an upshift in mobility on SDS-PAGE (although not as marked as with phosphorylation of Thr-412), and at least a partial restoration of the phosphorylation of Thr-252, as compared with its total absence in Thr-412 3 Ala (Fig. 5A). Although the degree of activation caused by Thr-412 3 Glu mutation is somewhat more marked in the absence of the carboxyl-terminal tail (data not shown), the activity of both p70 (Thr-412 3 Glu) and p70• CT104 (Thr-412 3 Glu) can be further increased by insulin, an effect attributable, at least in part, to the insulin-stimulated phosphorylation of Thr-252 (e.g. Fig. 5A).

Recently p70 (Ser-394) was shown to be a site of mitogen-regulated phosphorylation, wherein mutation greatly diminished 40 S kinase activity (10). We confirm the inhibitory effect of Ser-394 mutation on 40 S kinase activity and find that mutation of Ser-394 to Ala or Asp greatly inhibits phosphorylation at Thr-412 (Fig. 5B). Neither removal of the carboxyl-terminal tail nor mutation of Thr-412 to Glu restores 40 S kinase activ-

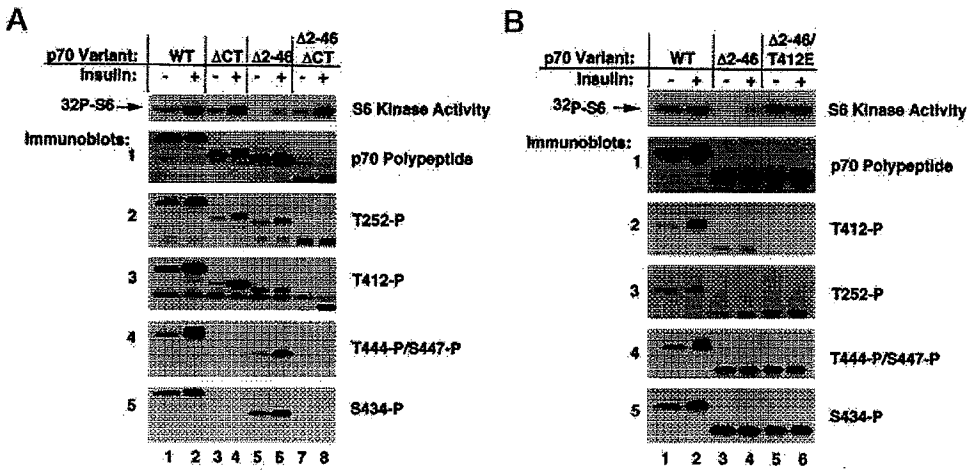

FIG. 4. The effects of p70 S6 kinase amino- and carboxyl-terminal truncation on the S6 kinase activity and site-specific phosphorylation of p70. A, CHO-IR cells were transfected with HA-tagged p70 wild type (WT, lanes 1 and 2); p70 deleted of the carboxyl-terminal tail, amino acids 422–525 (• CT, lanes 3 and 4); p70 deleted of amino acids 2–46 (• 2–46, lanes 5 and 6); and doubly deleted (• 2–46/• CT). Twelve hours after removal of serum, the cells were treated with carrier (lanes 1, 3, 5, and 7) or insulin 10^{-7} M, lanes 2, 4, 6, and 8) and extracted 10 min later. Anti-HA immunoprecipitates were analyzed for S6 kinase activity (^{32}P-S6) and by immunoblot using the antibodies indicated; type 2 anti-Thr-252(P) antibodies were used. ^{32}P cpm into S6: lane 1, 5953; lane 2, 19,517; lane 3, 3341; lane 4, 15,276; lane 5, 278; lane 6, 2579; lane 7, 3061; lane 8, 15,989. B, conversion of Thr-412 to Glu overcomes the inhibition engendered by the • 2–46 deletion. The experimental protocol was as in A. ^{32}P cpm into S6: lane 1, 3233; lane 2, 6937; lane 3, 427; lane 4, 1100; lane 5, 4057; lane 6, 5007.

ity to the Ser-394 3 Ala mutant (not shown), indicating that although Ser-394 influences Thr-412 phosphorylation in vivo, Ser-394 phosphorylation per se is required for p70 activity.

DISCUSSION

The goal of these studies was to characterize, in an intact cell, the changes in phosphorylation of a cohort of sites on the p70 S6 kinase in response to agonists and inhibitors and to correlate those changes with p70 catalytic activity. This analysis was carried out through the use of anti-p70 phosphopeptide antibodies, because the large number of data points examined would have rendered impractical such an analysis using conventional proteolysis and two-dimensional peptide mapping. Moreover, the residence of Thr-412 in a very hydrophobic domain has created difficulty in achieving reproducible tryptic/chymotryptic cleavage and recovery of this important site. Although the specificity of the antibodies employed has been clearly defined, the indirect nature of this analysis bears emphasis.

The sites chosen for study (Thr-252, Thr-412, Ser-434, Thr-444, and Ser-447) are a subset of those established by earlier work to be important in the regulation of p70 catalytic activity. Thus prior studies have shown that a cluster of sites in the p70 carboxyl-terminal tail (Ser-434, Ser-441, Ser-447, Ser-452, and Thr-444) (3–9), Thr-252 in the activation loop of the catalytic domain (8, 9, 11, 12, 16), and Ser-394 (10) and Thr-412 (9, 16), the latter two situated in a 65-amino acid segment immediately carboxyl-terminal to the catalytic domain, are each sites of insulin/mitogen-stimulated phosphorylation in vivo. Moreover, conversion of Thr-252, Thr-412, and Ser-394 to alanine each results in a • 90% decrease in p70 activity, and the simultaneous conversion of amino acids 434, 441, 444, and 447 to alanine also suppresses the activation of p70 by over 80%. Furthermore, conversion of Thr-412 to Glu increases "basal" p70 activity, i.e. activity in serum-deprived cells; independently, the selective phosphorylation of Thr-252 in vitro by PDK1 also increases p70 activity (11, 12). When these two modifications are combined, p70 activity is 20–30-fold greater than with either modification singly (11). Thus each of the phosphorylations chosen for study is of established importance in p70 regulation. In the present study, we sought to understand how the phosphorylation of these sites is regulated in vivo and how each contributes to changes in p70 activity. A dominant conclusion derived from these results is that although the regulation of the p70 carboxyl-terminal tail and the phosphorylation of Thr-252 in the activation loop are each crucial to p70 activation, it is the changes in the phosphorylation of Thr-412 that corresponds most closely with the fluctuations of p70 activity in vivo (Fig. 6).

The cluster of phosphorylation sites in the p70 carboxyl-terminal tail is situated in a pseudo-substrate autoinhibitory domain (3, 4), and it was inferred from the effects of mutation that multiple phosphorylation of these sites served to diminish the inhibitory potency of this segment by decreasing its ability to compete with the 40 S substrate for the catalytic domain (7). The present results uncover a separate, major mechanism of autoinhibition through the ability of the carboxyl-terminal tail to control access of upstream kinases to p70 phosphorylation sites crucial to activation, and in particular to Thr-412. The operation of the carboxyl-terminal tail as an inhibitor through this mechanism is revealed most clearly by deletion of p70 amino-terminal residues 2–46, which produces a profound inhibition of p70 that can be relieved by a further deletion of the carboxyl-terminal tail. Notably, the 2–46 deletion does not affect the phosphorylation of the carboxyl-terminal tail (at least at Ser-434, Thr-444, and Ser-447); however, the phosphorylation of Thr-412 is essentially abolished. Further deletion of the carboxyl-terminal tail restores Thr-412 phosphorylation and p70 activity. Alternatively, the need for Thr-412 phosphorylation can by bypassed by a Thr-412 3 Glu mutation, which, like the carboxyl-terminal deletion, overcomes the inhibitory effect of the • 2–46 deletion. The mechanism by which the p70 amino terminus controls the ability of the carboxyl-terminal tail to grant access to Thr-412 is unknown. The data in Fig. 5B and Ref. 10 indicate that the phosphorylation of Thr-412 is also dependent on the phosphorylation of Ser-394, another proline-directed site; it has not been determined as yet whether the • 2–46 deletion alters Ser-394 phosphorylation.

Just as the p70 tail appears to control access to Thr-412, the phosphorylation of Thr-412 is one of the critical regulators of Thr-252 phosphorylation; mutation of the Thr-412 to Ala abolishes phosphorylation of Thr-252 (Fig. 5A). Inasmuch as Thr-252 is a site whose phosphorylation is known to be required for

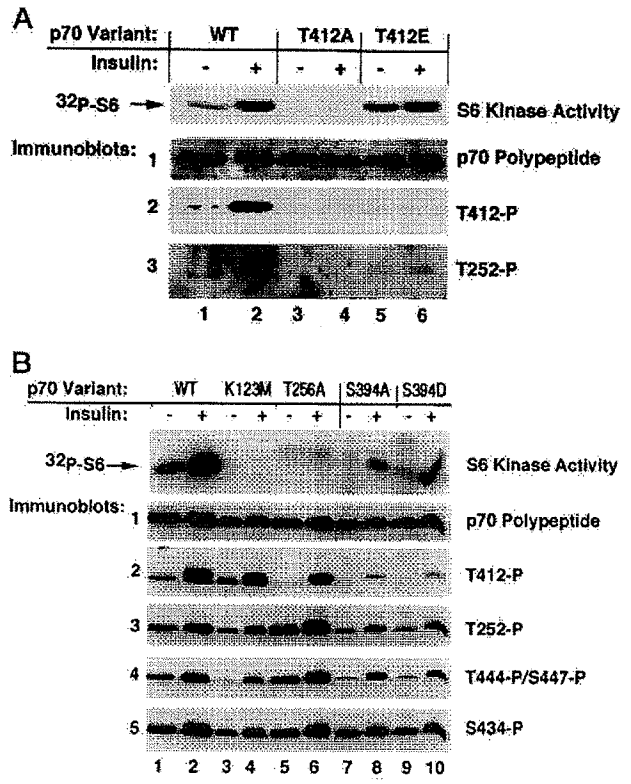

FIG. 5. The effect of various site-specific mutations on recombinant p70. A, mutation of Thr-412 modifies the phosphorylation of Thr-252 in vivo. CHO-IR cells expressing HA-tagged p70 wild type (WT, lanes 1 and 2), p70 Thr-412 3 Ala (T412A, lanes 3 and 4), and p70 Thr-412 3 Glu (T412E lanes 5 and 6) deprived of serum for 12 h and treated with carrier (lanes 1, 3 and 5) or insulin (10^{-7} M lanes 2, 4, and 6) for 10 min prior to extraction. Anti-HA immunoprecipitates were analyzed for S6 kinase activity (^{32}P-S6) and by immunoblot using the antibodies indicated; type 1 anti-Thr-252(P) antibodies were used. ^{32}P cpm into S6: lane 1, 1288; lane 2, 3852; lane 3, 60; lane 4, 86; lane 5, 2488; lane 6, 3516. B, the effect of mutations at Lys-123, Thr-256, and Ser-394 on p70 activity and site-specific phosphorylation. Serum-deprived CHO-IR cells expressing HA-tagged p70 wild type (WT, lanes 1 and 2), Lys-123 3 Met (K123M, lane 3 and 4), Thr-256 3 Ala (T256A, lanes 5 and 6), Ser-394 3 Ala (S394A, lanes 7 and 8), and Ser-394 3 Asp (S394D, lanes 9 and 10) were treated with carrier (lanes 1, 3, 5, 7, and 9) or insulin (10^{-7} M, lanes 2, 4, 6, 8, and 10) for 10 min prior to extraction; washed HA immunoprecipitates were analyzed for S6 kinase activity and by immunoblot using the antibodies indicated; type 2 anti-Thr-252(P) antibodies were used. ^{32}P cpm into S6: lane 1, 804; lane 2, 4299; lane 3, 7; lane 4, 22; lane 5, 18; lane 6, 170; lane 7, 286; lane 8, 469; lane 9, 310; lane 10, 907.

p70 activity, it could be argued that the effects of Thr-412 phosphorylation or p70 activity in vivo are achieved indirectly, through regulation of Thr-252. This cannot be entirely excluded until the effects of selective phosphorylation of Thr-412 has been determined. Nevertheless, it is clear that the activity of p70• CT104 (Thr-412 3 Glu) is substantially greater than p70• CT104, even after both polypeptides have been extensively dephosphorylated in vitro with protein phosphatase 2A(PP2A) (11). Moreover, the activity of PP2A-treated p70• CT104 (Thr-412 3 Glu) is comparable to that of p70• CT104 selectively phosphorylated at Thr-252 by PDK1, and the finding that the modification of both sites concurrently results in potent synergistic activation strongly supports the conclusion that the phosphorylation of Thr-412 provides an important direct contribution to p70 activation in addition to its influence on the phosphorylation of Thr-252 in vivo (11). Moreover, it is clear that the phosphorylation of Thr-412 is in some manner dependent on Thr-252, as conversion of this amino acid to alanine greatly suppressed Thr-412 phosphorylation.

Given that the concurrent phosphorylation of Thr-252 and Thr-412 appears to be necessary for p70 activation, the question remains as to whether the phosphorylation at both sites is coordinately regulated in vivo under all circumstances. The data presented here, especially in Figs. 2 and 3, address this issue. They demonstrate that in serum-deprived cells, basal phosphorylation of the Thr-252 is detectable, whereas Thr-412 appears dephosphorylated. Consequent to insulin addition, the phosphorylation at both these sites, as well as those in the carboxyl-terminal tail, increase concurrently with p70 activity. The coordinate phosphorylation of Thr-412 and Thr-252, however, is uncoupled in the presence of wortmannin and rapamycin. Both inhibitors cause dephosphorylation of p70 at all sites examined; however, the most rapid loss of phosphate occurs from Thr-412, followed closely by Thr-444/Ser-447, and the decrement in p70 kinase activity tracks directly with the loss of Thr-412(P) immunoreactivity. It is likely that the deactivation resulting from the selective Thr-412 dephosphorylation reflects the requirement for dual Thr-252/Thr-412 phosphorylation; however, this conclusion remains speculative in the absence of a selective inhibitor of Thr-252 phosphorylation. As to the mechanism underlying this rapid multisite dephosphorylation of p70, we infer that wortmannin, through the inhibition of PI-3 kinase, is deactivating the protein kinases responsible for p70 phosphorylation; direct evidence in support of this idea, however, is scant. The identity of the proline-directed kinases that act on p70 in vivo have not been unequivocally established; mitogen-activated protein kinases, stress-activated protein kinases, p38, and cdc2 can each phosphorylate some or all of these sites in vitro (5); the various Erks can be recruited through activation of PI-3 kinase in a cell- and stimulus-specific manner (17–19), and the actual effectors probably vary depending on the cell type and initiating stimulus, i.e. mitogens versus stress. PDK1, a candidate p70 Thr-252 kinase, appears to be constitutively active in vivo (21), and although it binds directly to PtdIns(3,4,5)P_3 in vitro, the lipid does not alter PDK1 catalytic activity. Thus wortmannin may inhibit Thr-252 phosphorylation either by delocalizing PDK1 from its site of action or by inhibiting the protein kinase acting on p70 (Thr-412). The p70 (Thr-412) kinase is probably activated by PtdIns(3,4,5)P_3 directly or indirectly, and the deactivation of Thr-412 phosphorylation may result in diminished phosphorylation or more rapid dephosphorylation of Thr-252.

The mechanism by which rapamycin promotes p70 Thr-412 dephosphorylation appears to be completely different than for wortmannin. Thus, whereas the S6 kinase activity and Thr-412 phosphorylation of the • 2–46/• CT104 variant are both inhibited by wortmannin, they are resistant to rapamycin (15, 16). This indicates that rapamycin does not inhibit the Thr-412 kinase; instead, the rapamycin-induced p70 Thr-412 dephosphorylation probably reflects rapamycin activation of a protein phosphatase whose activity is normally restrained by the active mTOR kinase. This view contrasts wtih the conclusions of Burnett et al. (20) who found that immunoprecipitates of mTOR (RAFT-1) catalyze phosphorylation recombinant fragments of p70 directly at Thr-412. We find such in vitro p70 Thr-412 phosphorylation by mTOR to be trivial and probably irrelevant, inasmuch as the activity of p70-(1–364) expressed in Sf9 cells is completely inhibited by rapamycin.

A prominent feature of the p70 immunoblots is the presence of multiple, closely spaced immunoreactive polypeptide bands. This ladder-like array of p70 polypeptides on SDS-PAGE was first observed in isolates of purified rat liver p70 polypeptides (22) and was shown subsequently to reflect different degrees of

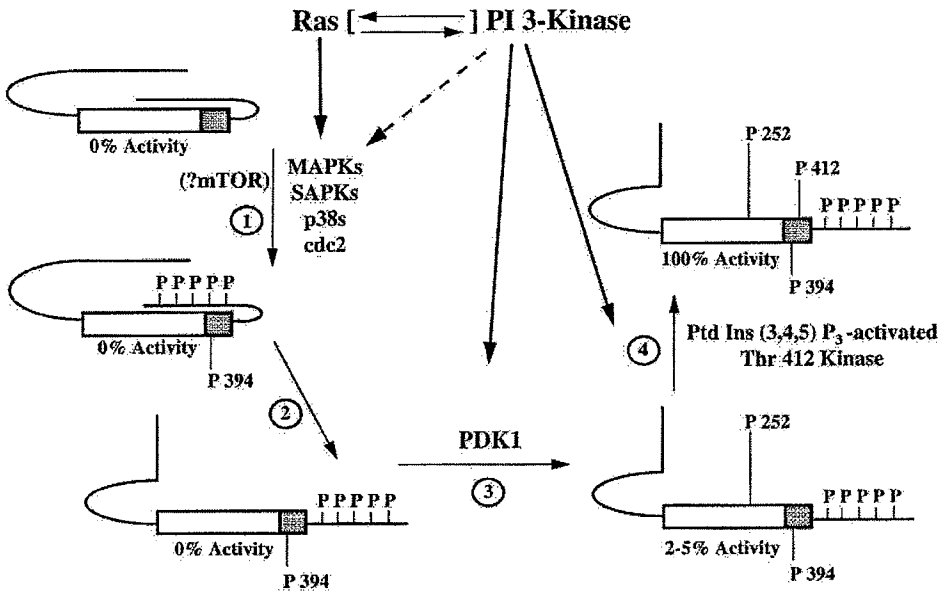

FIG. 6. A model for the insulin/mitogen activation of the p70 S6 kinase. Modified from Ref. 11. Step 1 involves the phosphorylation of an array of (Ser/Thr) Pro sites situated in the autoinhibitory domain in the carboxyl-terminal tail (Ser-434, Ser-441, Thr-444, Ser-447, and Ser-452) and in the catalytic domain extension (Thr-390 and Ser-394). A variety of proline-directed kinases, including various Erks and Cdc2 are capable of phosphorylating these sites in vitro (5), as is a proline-directed kinase activity associated with or intrinsic to mTOR. The identity of the kinases operative in vivo at this step is not known but depends in part on the cell type and stimulus. MAPK, mitogen-activated protein kinase; SAPK, stress-activated protein kinase. Step 2 involves the release of the phosphorylated carboxyl-terminal tail from the catalytic domain, enabling access of kinases to Thr-252 (11) and Thr-412 (Fig. 4). The existence of this step is inferred from the ability of the Δ2–46 (and Δ29–46) deletion to interrupt p70 activation at this point (see Fig. 4). Step 3 is the PDK1-catalyzed phosphorylation of Thr-252 in the activation loop of the catalytic domain, which increases p70 activity slightly, and sets up the conformation necessary for the concerted activation that occurs with dual Thr-252 and Thr-412 phosphorylation. Step 4 is the PtdIns(3,4,5)P_3-stimulated phosphorylation of Thr-412, which appears to be the final, rate-limiting step in p70 activation. The concurrent phosphorylation of Thr-252 and Thr-412 increases p70 activity by 20–30-fold over that resulting from the phosphorylation of either site singly (11). The deactivation of p70 that occurs on withdrawal of insulin or inhibition of PI-3 kinase results from the complete dephosphorylation of Thr-412, with residual phosphorylation remaining at Thr-252 (see Figs. 2B and 3B), and reflects the requirement for dual (412/252) phosphorylation. This basal state probably corresponds most closely to the form of p70 after Step 3, except with more dephosphorylation of the carboxyl-terminal tail.

p70 phosphorylation (14). The progressively slower mobility is not due primarily to the increasing negative charge engendered by multiple phosphorylation but to an altered conformation caused by phosphorylations at specific sites, particularly Thr-412 and Thr-252, which have a disproportionate effect on p70 mobility, presumably reflecting the importance of phosphorylation at those sites in determining p70 structure.

The transiently expressed recombinant p70 polypeptide, in contrast to the endogenous p70 polypeptides, always exhibits a large predominance of rapidly migrating p70 bands, with only a small minority of bands exhibiting retarded mobility after insulin or serum treatment in vivo. This reflects the substantial overexpression of the recombinant p70 polypeptides, to an extent that far exceeds the capacity of the upstream activating kinases, so that only a minority of the recombinant p70 polypeptides undergo full phosphorylation (as reflected by maximal slowing of mobility on SDS-PAGE) and activation, even in response to maximal stimulation by insulin. Based on the relative elution of immunoreactive p70 polypeptides and 40 S kinase activity on Mono Q chromatography, as well as the effects of phosphatase (in vitro) (14) and rapamycin (in vivo) on p70 activity and mobility on SDS-PAGE (22, 23), it was concluded previously that only the most slowly migrating (presumably) fully phosphorylated p70 polypeptides possessed "any" 40 S kinase activity.

The immunostaining of p70 by each of the anti-phosphopeptide antibodies is biased toward the visualization of bands of slower mobility. This pattern is readily observed in the anti-(Thr-252(P)), anti-(Thr-444(P)/Ser-447(P)), and anti-(Thr-434(P)) immunoblots, and is most pronounced in the anti-(Thr-412(P)) blots, which in general show only a single band, corresponding in mobility to the most slowly migrating band visualized by the other antibodies. The predominant association of Thr-412(P) immunoreactivity with the most slowly migrating bands, which correspond to the catalytically "active" p70 polypeptides, can now be interpreted in the context of the very powerful positive cooperativity between Thr-412(P) and Thr-252(P) in conferring 40 S kinase activity on the p70 polypeptide. It is this doubly modified p70 polypeptide that probably corresponds to the catalytically active fraction, which is found exclusively among the most slowly migrating p70 polypeptides generated in vivo. The present results indicate that Thr-252 is phosphorylated on p70 polypeptides of every mobility, the majority of which lack substantial 40 S kinase activity (for example, especially as seen in serum-deprived cells or after wortmannin or rapamycin inhibition). Nearly all immunoreactive p70 (Thr-412(P)) polypeptides are found among the most slowly migrating p70 polypeptides, probably because the Thr-412 phosphorylation can itself cause the upshift. The fraction of these Thr-412(P) polypeptides that are also phosphorylated at Thr-252 cannot be ascertained; however, those that are doubly modified will be at least 20–30-fold more active than those phosphorylated at Thr-412 only. Serum-deprived cells contain a reservoir of Thr-252-phosphorylated p70 polypeptides, not yet phosphorylated on Thr-412; inasmuch as Thr-252 phosphorylation appears to require Thr-412 phosphorylation, the presence of p70 Thr-252(P) but not Thr-412(P) in serum-deprived cells must reflect a differential sensitivity of these two sites to phosphatase as suggested by Fig. 2B. The ability of insulin and serum to increase the phosphorylation of Thr-252 likely reflects, in part, a prior phosphorylation of Thr-412. These considerations, especially the very low abundance of

p70 Thr-412(P) in serum-deprived or wortmannin/rapamycin-inhibited cells as compared with p70 Thr-252(P), indicate that it is the phosphorylation of Thr-412 that is the rate-limiting step in p70 activation. Presumably, it is also the last step in p70 activation (Fig. 6), although the concerted nature of the p70 multisite phosphorylation does not enable us to support this conclusion directly.

The identification of the p70 Thr-412 kinase remains one of the major unrealized goals necessary to complete the description of the apparatus interposed between PI-3 kinase and the p70 S6 kinase. The differences in the extent of phosphorylation at Thr-412 and Thr-252 in response to serum deprivation, rapamycin, wortmannin, as well as the ability to dissociate Thr-252 phosphorylation from Thr-412 phosphorylation in vivo through deletion of the carboxyl-terminal tail or conversion of Ser-394 to Ala all suggest that Thr-412 is phosphorylated in vivo by a different kinase than is Thr-252. This is further reinforced by the very marked selectivity of PDK1 for Thr-252 in vitro (11, 12), whereas Thr-252 and Thr-412 are phosphorylated with similar alacrity in vivo in response to insulin. A definitive answer requires the identification of a kinase specific for Thr-412, which is regulated by PI-3 kinase directly or indirectly, in a manner consistent with the patterns of insulin-stimulated p70 Thr-412 phosphorylation that occur in vivo, as described in this report.

Acknowledgment—We thank J. Prendable for preparation of the manuscript.

REFERENCES

1. Avruch, J. (1998) Mol. Cell Biochem. 182, 31–48
2. Sturgill, T. W., Ray, L. B., Erikson, E., and Maller, J. L. (1988) Nature 334, 715–718
3. Banerjee, P., Ahmad, M. F., Grove, J. R., Kozlosky, C., Price, D. U., and Avruch, J. (1990) Proc. Natl. Acad. Sci. U. S. A. 87, 8550–8554
4. Price, D. J., Mukhopadhyay, N. K., and Avruch, J. (1991) J. Biol. Chem. 266, 16281–16284
5. Mukhopadhyay, N. K., Price, D. J., Kyriakis, J. M., Pelech, S., Sanghera, J., and Avruch, J. (1992) J. Biol. Chem. 267, 3325–3335
6. Ferrari, S., Bannwarth, W., Morley, S. J., Totty, N. F., and Thomas G. (1992) Proc. Natl. Acad. Sci. U. S. A. 89, 7282–7286
7. Han, J.-W., Pearson, R. B., Dennis, P. B., and Thomas, G. (1995) J. Biol. Chem. 270, 21396–21403
8. Weng, Q.-P., Andrabi, K., Klippel, A., Kozlowski, M. T., Williams, L. T., and Avruch, J. (1995) Proc. Natl. Acad. Sci. U. S. A. 95, 5744–5748
9. Pearson, R. B., Dennis, P. B., Han, J. W., Williamson, N. A., Kozma, S. C., Wettenhall, R. E., and Thomas, G. (1995) EMBO J. 14, 5279–5287
10. Moser, B. A., Dennis, P. B., Pullen, N., Pearson, R. B., Williamson, N. A., Wettenhall, R. E., Kozma, S. C., and Thomas, G. (1997) Mol. Cell. Biol. 17, 5648–5655
11. Alessi, D., Kozlowski, M. T., Weng, Q.-P., Morrice, N., and Avruch, J. (1997) Curr. Biol. 8, 69–81
12. Pullen, N., Dennis, P. B., Andelkovic, M., Dufner, A., Kozma, S. C., Hemmings, B. A., and Thomas, G. (1998) Science 279, 707–710
13. Weng, Q.-P., Andrabi, K., Kozlowski, M. T., Grove, J. R., and Avruch, J. (1995) Mol. Cell. Biol. 15, 2333–2340
14. Grove, J. R., Banerjee, P., Balasubramanyam, A., Coffer, P. J., Price, D. J., Avruch, J., and Woodgett, J. R. (1991) Mol. Cell. Biol. 11, 5541–5550
15. Hara, K., Yonezawa, K., Weng, Q.-P., Kozlowski, M. T., Belham, C. T., and Avruch, J. (1998) J. Biol. Chem. 273, 14484–14494
16. Dennis, P. B., Pullen, N., Kozma, S. C., and Thomas, G. (1996) Mol. Cell. Biol. 16, 6242–6251
17. Cross, D. A. E., Alessi, D. R., and Vandenheede, J. R. (1994) Biochem. J. 303, 21–26
18. Lopez-Ilasaca, M., Crespo, P., Pellici, P. G., Gutkind, J. S., and Wetzker, R. (1997) Science 275, 394–397
19. Scott, P. H., and Lawrence, J. C., Jr. (1997) FEBS Lett. 409, 171–176
20. Burnett, P. E., Barrow, R. K., Cohen, N. A., Snyder, S. H., and Sabatini, D. M. (1998) Proc. Natl. Acad. Sci. U. S. A. 95, 1432–1437
21. Alessi, D. R., James, S. R., Downes, C. P., Holmes, A. B., Gafrey, P. R. J., Reese, C. B., and Cohen, P. (1997) Curr. Biol. 7, 261–269
22. Price, D. J., Nemenoff, R. A., Avruch, J. (1989) J. Biol. Chem. 264, 13825–13833
23. Price, D. J., Grove, J. R., Calvo, V., Avruch, J., and Bierer, B. E. (1992) Science 257, 973–977
24. Chung, J., Kuo, C. J., Crabtree, G. R., and Blenis, J. (1992) Cell 69, 1227–1236